INVESTIGATING THE EFFECT OF MEMBRANE ANCHORING ON PHOTO-INDUCED ELECTRON TRANSFER PYRAZOLINE BASED FLUORESCENT PROBES

A Thesis

Presented to

The Academic Faculty

By

Jonathan Hofmekler

In Partial Fulfillment

of the Requirements for the Degree

Master of Science in the

School of Chemistry and Biochemistry

Georgia Institute of Technology

December 2011

INVESTIGATING THE EFFECT OF MEMBRANE ANCHORING ON PHOTO-INDUCED ELECTRON TRANSFER PYRAZOLINE BASED FLUORESCENT PROBES

Approved by:

Prof. Christoph J. Fahrni

School of Chemistry and Biochemistry

Georgia Institute of Technology

Dr. Wendy L. Kelly

School of Chemistry and Biochemistry

Georgia Institute of Technology

Dr. Adegboyega K. Oyelere

School of Chemistry and Biochemistry

Georgia Institute of Technology

Date Approved: Novemeber 11, 2011

ACKNOWLEDGEMENTS

First and foremost I would like to thank my advisor, Prof. Christoph J. Fahrni for supporting this work. M. Thomas Morgan and Sumalekshmy are thanked for their help and expertise regarding synthesis and fluorescence measurements. Pritha Bagchi is thanked for her cell imaging data and pK_a measurements assistance and Rachel Bennett is thanked for her high resolution electron spray ionization mass spectrometry data for the final compounds.

TABLE OF CONTENTS

LIST OF TABLES

LIST OF FIGURES

LIST OF SCHEMES

LIST OF ABBREVIATIONS

Abbreviation or Symbol	Term
µL	Microliter
µM	Micromolar
A	Acceptor
A^*	Excited acceptor
$A^{\bullet -}$–$D^{\bullet +}$	Radical ion pair
abs	Absorption
BODIPY	Boron dipyrromethene
BSC	Bathocuproine disulfonate
cm	Centimeter
D	Donor
DMEM	Dulbecco's modified eagle medium
DMF	Dimethyl formamide
DMSO	Dimethylsulfoxide
$E(A^-/A)$	Acceptor ground state reduction potential
$E(D/D^+)$	Donor ground state reduction potential

E_{00}	Excited state equilibrium energy
em	Emission
eq	Equivalent
ET	Electron transfer
f_e	Fluorescence enhancement factor
g	Gram
GS	Ground state
h	Hour
HOMO	Highest occupied molecular orbital
HPLC	High pressure liquid chromatography
IC	Internal conversion
k_{cr}	Rate constant for charge recombination process
k_{et}	Rate constant for electron transfer
k_{nr}	Rate constant for non radiative process
k_r	Rate constant for radiative process
LA-ICP-MS	Laser ablation inductively coupled plasma-mass spectrometry
LUMO	Lowest unoccupied molecular orbital

m/z	Mass over charge ratio
MeCN	Acetonitrile
mg	Miligram
mM	Millimolar
MOPS	3-morpholinopropane-1-sulfonic acid
MS	Mass spectrometry
MTBE	Methyl-*tert* butylether
nm	Nanometer
NMR	Nuclear magnetic resonance
PET	Photoinduced electron transfer
PIPBS	Piperazine-N,N'-bis(4-butanesulfonic acid)
PIPES	Piperazine-N,N′-bis(2-ethanesulfonic acid)
ppm	Parts per million
S_1	First singlet excited state
SXRF	Synchrotron X-ray fluorescence
THF	Tetrahydrofuran
TLC	Thin layer chromatography

UV-vis	Ultra-violet visible
w_p	Coulomb stabilization energy associated with the intermediate radical ion pair
ΔG_{et}	Gibbs free energy change for electron transfer
Φ	Quantum yield

SUMMARY

Fluorescence microscopy is a powerful analytical tool for visualizing biological processes at the subcellular level. In this regard, 1,3,5-triarylpyrazoline based fluorescent probes which act as “turn-on” probes, have been extensively researched. These probes achieve their fluorescence “turn-on” response by inhibition of fluorescence quenching by acceptor-excited photoinduced electron transfer upon binding of an analyte. It has been recently shown that some fluorescent probes used in biological research form colloids composed of nanoparticles, due to their hydrophobic character. This hydrophobic character can also lead to partitioning of the probe into cellular membranes. Colloid formation and membrane partitioning may affect the probes’ photophysical properties such as absorption and emission wavelength and quantum yields. Recently, a series of 1,3,5-triarylpyrazolines synthesized in our group by M. T. Morgan, showed no formation of aggregates in aqueous buffer. Surprisingly, these probes increased their fluorescence intensity in the presence of liposomes. The photoinduced electron transfer process is greatly affected by the polarity of the medium in which the probe is used. In this study, the effect of membrane proximity on the photoinduced electron transfer process for pyrazoline based “turn-on” probes has been investigated. A series of water soluble 1,3,5-triarylpyrazolines have been synthesized in which a *N*,*N*-dialkylaniline moiety acts as an electron donor and a proton acceptor and an alkylated sulfonamide moiety acts as a molecular anchor for interaction with neutral and anionic liposomes.

CHAPTER 1

INTRODUCTION

1.1 Introduction

Transition metals are essential for sustaining all forms of life. Approximately one third of all known proteins contain one or more metal cations in their active site.[1] To ensure proper maintenance of this metal ion pool at the cellular level, nature has developed sophisticated regulatory mechanisms that involve a complex interplay of DNA with proteins and other biomolecules.[2] Over the past decade, metal dyshomeostasis has been associated with a growing number of diseases, including the genetic disorders Wilson's disease[3] and Menkes syndrome[4] and the neurodegenerative diseases Alzheimer's disease[5] and Parkinson's disease[6]. While some progress has been made towards understanding the molecular basis of these disorders, many important questions remain unanswered. For example, little is known about the regulatory mechanisms involved in metal ion transport, storage, and trafficking or about the recycling pathways of metal ions upon protein degradation. A better understanding of these processes is critical to create new ways of treating disorders related to metal dyshomeostasis.

There are currently several highly sensitive micro-analytical techniques and instruments available for the *in situ* detection of metal ions.[2a] For example, laser ablation-inductively coupled plasma-mass spectrometry (LA-ICP-MS) and synchrotron X-ray fluorescence (SXRF) can provide quantitative topographical maps of trace metals. These methods, however, are not suitable for continuous imaging of live cells due to their use of high-energy ion beams and ionizing x-rays, respectively. In contrast, fluorescence

microscopy represents a powerful and noninvasive analytical tool, which under favorable conditions, and depending on the brightness of the fluorescent probe, is capable of visualizing biological processes even at the single molecule level.[7] It is important to note that metal cations are not inherently fluorescent. At present, fluorescent probes have been developed for many biologically relevant nonredox-active and redox-active metal cations including Ca^{2+}, Cd^{2+}, Hg^{2+}, Mg^{2+}, Zn^{2+}, $Cu^{1+/2+}$ and $Fe^{2+/3+}$ and for monitoring differences in intracellular pH levels.[8] Depending on their fluorescence response upon binding of the analyte, the probes can be grouped into two classes: ratiometric probes which undergo a spectral shift of the excitation or emission wavelength, and "turn-on" probes which respond with a change in fluorescence intensity.

Fluorescent probes designed for biological research must maintain a balance between hydrophilicity and hydrophobicity. If the probe is too hydrophilic, it may not passively diffuse through the lipid bilayer membrane of the targeted cell. On the other hand, if the probe is too hydrophobic, it may either partition into the lipid membrane or form aggregates. Both phenomena have dramatic effects on the photophysical properties of the fluorescent probes.

1.2 Fundamental concepts of fluorescence

In order for fluorescence to occur, a fluorophore must first absorb a photon, which results in promotion of an electron from an occupied molecular orbital, typically the highest occupied molecular orbital, HOMO, to an unoccupied molecular orbital, typically the lowest unoccupied molecular orbital, LUMO, (Figure 1.1a).[9] Upon excitation the fluorophore arrives at a vibrationally excited state of the first excited electronic sate, (S_1).

After rapid relaxation to the vibrational ground state of the first excited electronic state, the molecule returns to the electronic ground state, (GS), while simultaneously emitting a photon, (Figure 1.1b).[9] It is important to note that the emitted photon is lower in energy compared to the absorbed photon due to energy loss during the vibrational relaxation process. In addition, the excited state can undergo several non-radiative processes such as internal conversion or intersystem crossing (Figure 1.1b).[9] The ratio between the rate constant of the radiative process (k_r) and the rate constants of all radiative and non-radiative processes ($k_r + k_{nr}$) corresponds to the quantum yield, $\Phi = \left(\frac{k_r}{k_r+k_{nr}}\right)$. The quantum yield could be regarded as the fluorescence efficiency. If the non-radiative process is faster than the radiative process, then the radiative process is less likely to occur, resulting in fluorescence quenching and a reduced quantum yield.

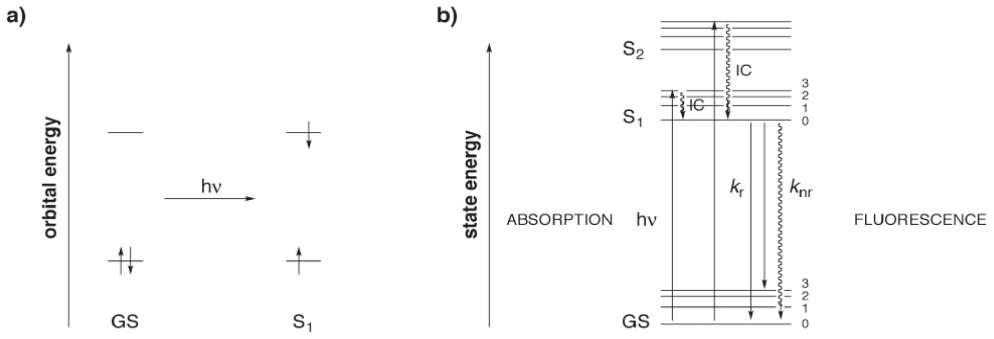

Figure 1.1: Photo-excitation of a fluorophore. a) orbital energy diagram, b) Jablonski diagram.
GS = ground state, S_1 = first excited singlet state, IC = internal conversion, k_r = radiative rate constant, k_{nr} = non-radiative rate constant.

The fluorescence response of fluorescent probes is modulated through several different mechanisms, including (n-π*)/(π-π*) excited state inversion, photoinduced charge transfer, excited state intramolecular proton transfer, and photoinduced electron transfer.

1.3 Acceptor-excited photoinduced electron transfer and 1,3,5-triarylpyrazolines

A large class of cation responsive fluorescence "turn-on" probes utilizes acceptor-excited photoinduced electron transfer (PET) as a quenching mechanism to modulate the fluorescence emission.[9] Upon excitation, the fluorophore (A*) is rendered a strong oxidant, and in proximity of a suitable donor/receptor moiety (D), an electron transfer may occur to form the corresponding radical ion pair ($A^{\bullet -}$–$D^{\bullet +}$). This radical ion pair typically undergoes a rapid non-radiative charge recombination with rate constant k_{cr} back to the ground state, (Figure 1,2a).[9] As a result, PET quenches the fluorescence and decreases the quantum yield. If the electron donor moiety is protonated or a metal cation is coordinated to it, the PET process is rendered thermodynamically less favorable, resulting in an increase of fluorescence intensity and quantum yield (Figure 1.2b). Because the analyte interacts directly with the donor/receptor moiety and not with the fluorophore, the emission wavelength is unchanged and only the emission intensity is altered.

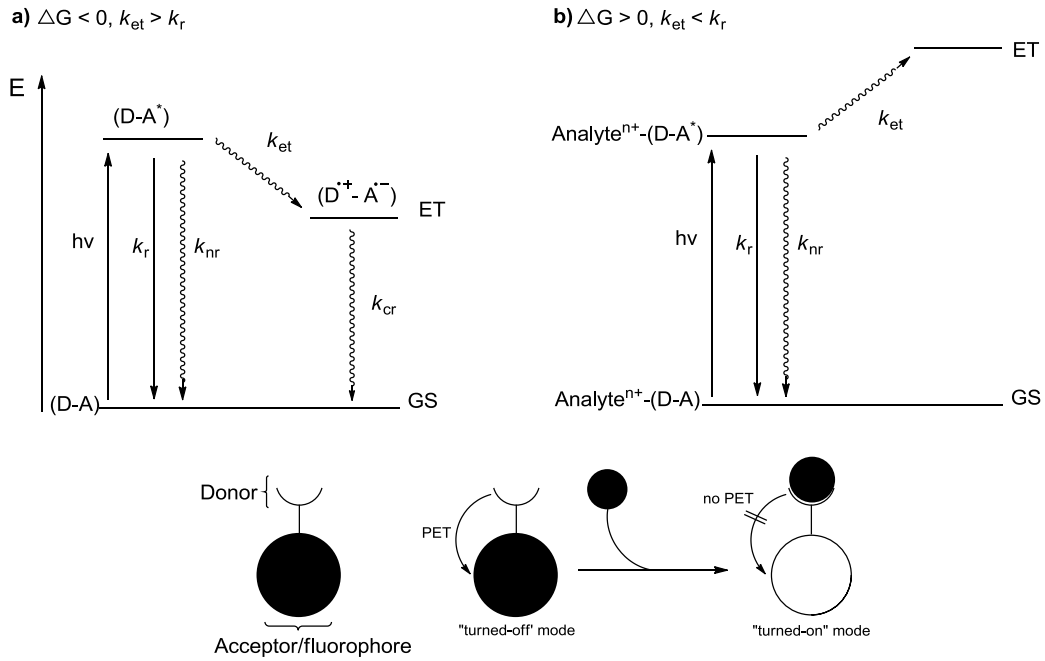

Figure 1.2: Photoinduced electron transfer switching mechanism. a) In the absence of the analyte, electron transfer from the donor D to the excited fluorophore A^* is thermodynamically favorable. The rate of electron transfer k_{et} is faster than the rate for the radiative process, k_r, resulting in emission quenching. b) Analyte coordination to the electron donor D decreases the driving force for PET, and slows down the electron transfer process. The radiative process favorably competes with PET, and the fluorescence is turned on. GS = groundstate, ET = electron transfer state.

To create a fluorescence "turn-on" probe which takes advantage of PET, one must ensure that the fluorescence properties of the probe will not change due to an analyte-mediated quenching pathway. This quenching pathway commonly occurs with redox-active cations such as Cu(I) in the case of bathocuproine disulfonate (BSC)[10]. This can be achieved by electronically decoupling the analyte binding moiety from the fluorophore by introducing a spacer between them. In this regard, 1,3,5-triarylpyrazolines have been extensively studied due to their unique electronic structure shown in Figure 1.3.[11] As illustrated with the orbital density plots of the 1,3,5-triphenylpyrazoline, the HOMO is located in the 1-aryl ring and the LUMO is located on the 3-aryl ring, which means that the fluorophore moiety is composed of the conjugated π system containing the 1-aryl

ring and the 3-aryl ring. The 5-aryl ring is electronically decoupled from the 1- and 3-aryl rings by an sp^3 hybridized carbon.

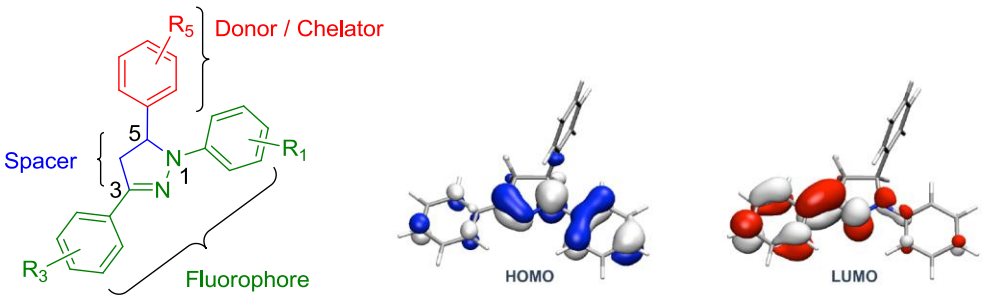

Figure 1.3: Photoinduced electron transfer probes based on 1,3,5-triarylpyrazoline fluorophores. Left: molecular architecture. Right: HOMO (left) and LUMO (right) densities of 1,3,5-triphenylpyrazoline.

In absence of the analyte, the PET quenching process must be a spontaneous process for a probe to act as a "turn-on" probe, therefore, the electron transfer process must be exergonic. The free energy change of PET can be estimated based on the Rehm-Weller equation [12]

$$\Delta G_{et} = E(D^+/D) - E(A^-/A) - \Delta E_{00} + w_p \qquad (1.1)$$

In this equation ΔG_{et} is the Gibb's free energy change. $E(D^+/D)$ and $E(A^-/A)$ represent the donor and acceptor ground state reduction potentials respectively. ΔE_{00} is the excited state equilibrium energy, and w_p is the Coulomb stabilization energy associated with the intermediate radical ion pair. Because the HOMO and the LUMO densities of 1,3,5-triarylpyrazoline fluorophores are unequally distributed with regard to the two 1- and 3-aryl substituents, it is possible to adjust ΔE_{00} without significantly altering $E(A^-/A)$ and *vice versa*. More specifically, an electron withdrawing substituent on the 1-aryl ring

preferentially lowers the HOMO energy, and thus increases ΔE_{00}, while an electron withdrawing substituent on the 3-aryl ring renders the reduction potential $E(A^{-}/A)$ more favorable.

A very important factor affecting ΔG_{et} is the polarity of the medium in which the probes are used. Specifically, a polar solvent will favor the formation of an ionic electron transfer state ($A^{\bullet -}$–$D^{\bullet +}$) from the neutral excited state (A^{*}-D). The oxidation potential of the donor and reduction potential of the acceptor along with the work term, w_p may change dramatically when switching from a polar to a non-polar solvent. In a non-polar solvent the oxidation potential will become more positive and the reduction potential will become more negative (compared to a polar environment), requiring more energy to remove an electron from the donor moiety and more energy to add an electron to the acceptor moiety. On the other hand, the work term contribution to the free energy change will increase in a non-polar solvent. This increase is typically not sufficient so to compensate for the less favorable potentials. Therefore, to optimize the contrast between the free and analyte bound form of a probe, ΔG_{et} must be specifically tuned with regard to the polarity of the surrounding medium (solvent). This is of vital importance because most fluorescent probes used in biological research are lipophilic and tend to form aggregates in aqueous media or partition into the phospholipid bilayer membrane.

1.4 Aggregation and membrane partitioning of fluorescent probes

Fluorescent probes must be sufficiently hydrophilic to dissolve in biological buffers, but lipophilic enough to reach the cellular targets by passive diffusion across the

plasma membrane[7c]. If a fluorescent probe is too lipophilic it will partition into the lipid bilayer or aggregate in aqueous solution, both of which may dramatically alter the photophysical properties including, quantum yield, absorption and emission wavelengths[13]. For example, boron dipyrromethene (BODIPY) fluorescent probes tend to form J and H aggregates in polar solvent that exhibit dramatically different photophysical properties compared to their non-aggregated forms.[14] Even BODIPY probes which were functionalized with water solubilizing groups showed a dramatic increase in quantum yield when an organic co-solvent (DMSO) was added to an aqueous solution of the dye.[15]

Because most fluorescent probes used in biological research are lipophilic and poorly water soluble, a very common procedure of applying them to cells is to create a DMSO stock solution and dilute it into the aqueous buffer to achieve a final probe concentration in the low micromolar range. A recent study conducted in our group by Morgan *et al*.[16], showed that this approach did produce optically clear solutions, but those solutions contained nanoparticles of sizes below the diffraction limit, as indicated by dynamic light scattering experiments (Table 1.1). Although formation of such colloidal aggregates might not necessarily invalidate the biological studies utilizing these probes, the photophysical properties of the colloid may be dramatically different compared to those of the monomeric form. The cellular environment is likely to induce a shift in the equilibrium between the aggregated and monomeric forms of the probe. Hence, when using fluorescent probes in the mixed polarity of the cell, one must practice caution when analyzing the results.

Table 1.1: Colloid formation of Cu(I)-selective fluorescent probes in aqueous buffer (10 mM MOPS/K^+, pH 7.2, 25° C)[a]

Probe	Rh(nm)[b]	SD(nm)[c]
1	100	12
CS1	49	6
CS3	67	9
CTAP-1[d]	63	6

[a]DMSO stock solution (1 mM) of the probe diluted into aqueous buffer to a final concentration of 5 µM. [b]Hydrodynamic radius. [c]Standard deviation. [d]Potassium salt.

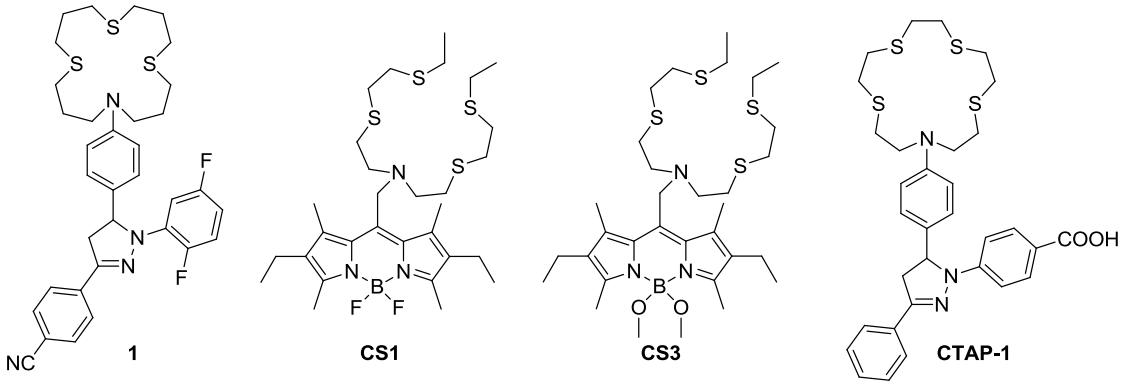

Figure 1.4: Previously published Cu(I)-selective fluorescence probes.[16]

The probes shown in Figure 1.4 were functionalized with a thioether crown to selectively bind Cu(I). This thioether crown further increases their lipophilic character. While probes **1**, **CS1** and **CS3** have no water solubilizing functional groups to mitigate their lipophilicity, **CTAP-1** has been functionalized with a carboxylic acid on its 1-aryl ring. Surprisingly, dynamic light scattering experiments revealed that **CTAP-1** still forms aggregates.

A series of triarylpyrazolines, utilizing acceptor excited photoinduced electron transfer as a quenching mechanism for modulating fluorescence response, were

synthesized by Morgan *et al*. (Figure 1.5). When dissolved in aqueous buffer, these compounds produced aggregate-free solutions; however, in the presence of liposomes a significant increase in fluorescence intensity was observed. This unexpected observation suggests that the hydrophilic probes still interact with the lipophilic environment of the lipid bilayer, which in turn renders the PET process thermodynamically less favorable, resulting in increase of quantum yield.

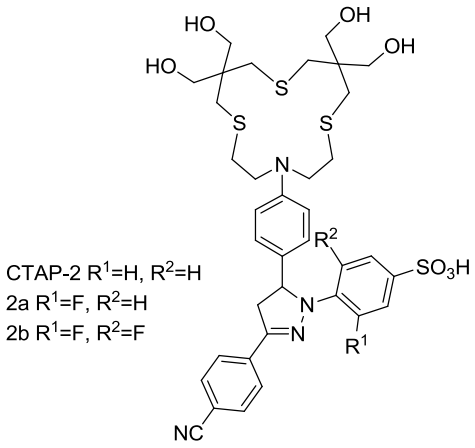

Figure 1.5: Structures of 1,3,5-triarylpyrazolines that do not aggregate, but in presence of liposomes show a significant increase in fluorescence intensity.

Based on the dynamic light scattering experiments, it is likely that probes **1**, **CS1** and **CS3** exhibit sufficient lipophilic character to become completely embedded in the phospholipid bilayer of the liposome. It was expected that the anionic charge on the 1-aryl ring on **CTAP-1** would cause some repulsion between the aryl ring and the phospholipid head groups in the lipid bilayer. Nevertheless, the 3- and 5-aryl rings appear to be sufficiently lipophilic to partition within the membrane. In the case of **CTAP-2**, interaction with the lipid bilayer is expected to be reduced compared to the other more lipophilic probes due to the presence of water solubilizing groups on the thioether crown

and the 1-aryl ring. Still, the 3-aryl ring and its nitrile substituent along with the carbon framework that constitutes the spacer between the fluorophore and the thioether crown are lipophilic enough to promote membrane interactions throughout that region of the molecule. Because the interaction of the probes with the lipid bilayer is not well defined, it is nearly impossible to estimate the effect of membrane proximity on the kinetics of the PET process. Because a decrease in the PET kinetics results in a quantum yield increase, the photophysical properties provide a direct readout to gauge changes in the PET kinetics.

A study on characterizing, in a well-defined manner, the effect of phospholipid bilayer membrane proximity on 1,3,5-triarlypyrazoline-based fluorescence "turn-on" probes is presented herein.

REFERENCES

1. Fahrni, C. J., Fluorescent probes and labels for cellular imaging. *CHIMIA International Journal for Chemistry* **2009,** *63* (11), 714-720.
2. (a) McRae, R.; Bagchi, P.; Sumalekshmy, S.; Fahrni, C. J., In situ imaging of metals in cells and tissues. *Chemical Reviews* **2009,** *109* (10), 4780-4827; (b) Finney, L. A.; O'Halloran, T. V., Transition metal speciation in the cell: insights from the chemistry of metal ion receptors. *Science* **2003,** *300* (5621), 931-936.
3. Pfeiffer, R. F., Wilson's disease. *Seminars in Neurology* **2007,** *27* (02), 123,132.
4. Tumer, Z.; Moller, L. B., Menkes disease. *European Journal Human Genetics* **2010,** *18* (5), 511-518.
5. Bonda, D. J.; Lee, H.-g.; Blair, J. A.; Zhu, X.; Perry, G.; Smith, M. A., Role of metal dyshomeostasis in Alzheimer's disease. *Metallomics* **2011,** *3* (3), 267-270.
6. Tougu, V.; Tiiman, A.; Palumaa, P., Interactions of Zn(II) and Cu(II) ions with Alzheimer's amyloid-beta peptide. Metal ion binding, contribution to fibrillization and toxicity. *Metallomics* **2011,** *3* (3), 250-261.
7. (a) de Silva, A. P.; Moody, T. S.; Wright, G. D., Fluorescent PET (photoinduced electron transfer) sensors as potent analytical tools. *Analyst* **2009,** *134* (12), 2385-2393; (b) Tsien, R. Y., Fluorescent probes of cell signaling. *Annual Review of Neuroscience* **1989,** *12* (1), 227-253; (c) Domaille, D. W.; Que, E. L.; Chang, C. J., Synthetic fluorescent sensors for studying the cell biology of metals. *Nature Chemical Biololgy* **2008,** *4* (3), 168-175.
8. (a) Grynkiewicz, G.; Poenie, M.; Tsien, R. Y., A new generation of Ca^{2+} indicators with greatly improved fluorescence properties. *Journal of Biological*

Chemistry **1985,** *260* (6), 3440-3450; (b) Kim, H. M.; Seo, M. S.; An, M. J.; Hong, J. H.; Tian, Y. S.; Choi, J. H.; Kwon, O.; Lee, K. J.; Cho, B. R., Two-photon fluorescent probes for intracellular free zinc ions in living tissue. *Angewandte Chemie* **2008,** *120* (28), 5245-5248; (c) Komatsu, H.; Iwasawa, N.; Citterio, D.; Suzuki, Y.; Kubota, T.; Tokuno, K.; Kitamura, Y.; Oka, K.; Suzuki, K., Design and synthesis of highly sensitive and selective fluorescein-derived magnesium fluorescent probes and application to intracellular 3D Mg^{2+} imaging. *Journal of the American Chemical Society* **2004,** *126* (50), 16353-16360; (d) Lu, C.; Xu, Z.; Cui, J.; Zhang, R.; Qian, X., Ratiometric and highly selective fluorescent sensor for cadmium under physiological pH range: a new strategy to discriminate cadmium from zinc. *The Journal of Organic Chemistry* **2007,** *72* (9), 3554-3557; (e) Zeng, L.; Miller, E. W.; Pralle, A.; Isacoff, E. Y.; Chang, C. J., A selective turn-on fluorescent sensor for imaging copper in living cells. *Journal of the American Chemical Society* **2005,** *128* (1), 10-11; (f) Fan, L.-J.; Jones, W. E., A highly selective and sensitive inorganic/organic hybrid polymer fluorescence "turn-on" chemosensory system for iron cations. *Journal of the American Chemical Society* **2006,** *128* (21), 6784-6785; (g) Takahashi, A.; Zhang, Y.; Centonze, E.; Herman, B., Measurement of mitochondrial pH in situ. *BioTechniques* **2001,** *30* (4).

9. (a) Kavarnos, G. J., *Fundamentals of photoinduced electron transfer*. VCH Publishers: United States of America, 1993; (b) Fahrni, C. J., Design of cation-selective synthetic fluorescent indicators in chemosensors, John Wiley & Sons, Inc.: 2011; pp 371-394.

10. Rapisarda, V. A.; Volentini, S. I.; Farías, R. N.; Massa, E. M., Quenching of bathocuproine disulfonate fluorescence by Cu(I) as a basis for copper quantification. *Analytical Biochemistry* **2002,** *307* (1), 105-109.

11. (a) Verma, M.; Chaudhry, A. F.; Morgan, M. T.; Fahrni, C. J., Electronically tuned 1,3,5-triarylpyrazolines as Cu(I)-selective fluorescent probes. *Organic & Biomolecular Chemistry* **2010,** *8* (2), 363-370; (b) Cody, J.; Mandal, S.; Yang, L.; Fahrni, C. J., Differential tuning of the electron transfer parameters in 1,3,5-triarylpyrazolines: a rational design approach for optimizing the contrast ratio of fluorescent probes. *Journal of the American Chemical Society* **2008,** *130* (39), 13023-13032; (c) Chaudhry, A. F.; Verma, M.; Morgan, M. T.; Henary, M. M.; Siegel, N.; Hales, J. M.; Perry, J. W.; Fahrni, C. J., Kinetically controlled photoinduced electron transfer switching in Cu(I)-responsive fluorescent probes. *Journal of the American Chemical Society* **2009,** *132* (2), 737-747; (d) Fahrni, C. J.; Yang, L.; VanDerveer, D. G., Tuning the photoinduced electron-transfer thermodynamics in 1,3,5-triaryl-2-pyrazoline fluorophores: X-ray structures, photophysical characterization, computational analysis, and in vivo evaluation. *Journal of the American Chemical Society* **2003,** *125* (13), 3799-3812; (e) Lin, J.; Rivett, D.; Wilshire, J., The preparation and photochemical properties of some 1,3-Diphenyl-2-pyrazolines containing a heteroaromatic substituent. *Australian Journal of Chemistry* **1977,** *30* (3), 629-637; (f) Rivett, D.; Rosevear, J.; Wilshire, J., The preparation and spectral properties of some monosubstituted 1,3,5,-Triphenyl-2-pyrazolines. *Australian Journal of Chemistry* **1979,** *32* (7), 1601-1612.

12. Rehm, D. W., A., Kinetics of fluorescence quenching by electron and H-atom transfer. *Israel Journal of Chemistry* **1970,** *8,* 259-271.

13. Karolin, J.; Johansson, L. B. A.; Strandberg, L.; Ny, T., Fluorescence and absorption spectroscopic properties of dipyrromethene boron difluoride (BODIPY) derivatives in liquids, lipid membranes, and proteins. *Journal of the American Chemical Society* **1994,** *116* (17), 7801-7806.

14. Li, L.; Han, J.; Nguyen, B.; Burgess, K., Syntheses and spectral properties of functionalized, water-soluble BODIPY derivatives. *The Journal of Organic Chemistry* **2008,** *73* (5), 1963-1970.

15. Niu, S. L.; Ulrich, G.; Ziessel, R.; Kiss, A.; Renard, P.-Y.; Romieu, A., Water-soluble BODIPY derivatives. *Organic Letters* **2009,** *11* (10), 2049-2052.

16. Morgan, M. T.; Bagchi, P.; Fahrni, C. J., Designed to dissolve: suppression of colloidal aggregation of Cu(I)-selective fluorescent probes in aqueous buffer and in-gel detection of a metallochaperone. *Journal of the American Chemical Society* **2011,** *133* (40), 15906-15909.

CHAPTER 2

SYNTHESIS AND CHARACTERIZATION OF NEW WATER-SOLUBLE 1,3,5-TRIARLYPYRAZOLINE BASED FLUORESCENT PROBES

2.1 Introduction

To systematically characterize the proximity effect of a lipid bilayer on photoinduced electron transfer (PET) based probes, a series of water-soluble 1,3,5-triarylpyrazoline derivatives **9**-**11** with varying degrees of lipophilicity were synthesized. A metal ion receptor might potentially complicate the fluorescence quenching behavior, through formation of ternary complexes with solvent molecules as recently demonstrated by Chaudhry *et al.*[1] Therefore, a simple *N*,*N*-dialkylaniline moiety was chosen as a representative electron donor and proton acceptor to modulate PET (Figure 2.1). Water solubility was achieved by attaching a sulfonic acid group to the 1-aryl ring and by functionalizing the 3- and 5-aryl rings with a total of three carboxylic acid groups. To tune the lipophilicity and degree of membrane association, the sulfonamide moiety of the 3-aryl ring was extended with linear alkyl chains of varying lengths.

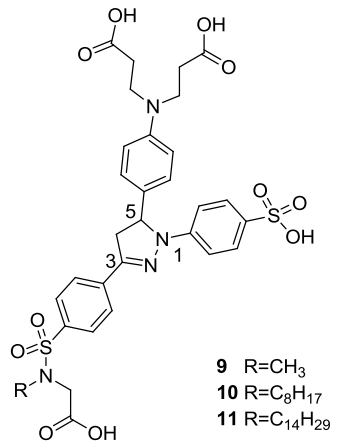

Figure 2.1: Structure of 1,3,5 triarylpyrazolines **9**-**11**.

As mentioned in the previous chapter, the 5-aryl ring of 1,3,5-triarylpyrazolines is electronically decoupled from the fluorophore and can act as a donor/receptor moiety. Upon protonation, the donor potential of the aniline moiety increases, thus resulting in a thermodynamically less favorable PET process. By positioning the alkyl-chain at the 3-aryl sulfonamide group, the interaction with the lipid biplayer can be expected to occur in a well-defined manner. Furthermore, anionic water-solubilizing groups were distributed throughout the pyrazoline skeleton to avoid membrane association with other regions of the pyrazoline framework as indicated in Chapter 1 for **CTAP-1** and **CTAP-2**.

2.2 Synthesis

The first report on the synthesis of 1,3,5-triarylpyrazolines dates back more than a century.[2] Since then, the pyrazoline core has been commonly constructed by condensation of a chalcone and phenylhydrazine derivative carrying the corresponding substituents.[1, 3] The synthesis in this work followed accordingly; the key intermediate in the synthesis of derivatives **9-11** was chalcone **4**, which was obtained by a Claisen-

Schmidt condensation of aldehyde **2** and acetophenone derivative **3**, (Scheme 2.1). To minimize the undesired Michael addition between the formed chalcone and unreacted starting material, aldehyde **2** was used with a two-fold excess. Aldehyde **2** was obtained in 70% overall yield, starting from unsubstituted aniline that was subjected to a double Michael addition with excess ethyl acrylate, and followed by Vilsmeier-Haack formylation with phosphoryl chloride in dimethyl formamide. The acetophenone derivative **3** was readily accessible by coupling of ethyl glycinate with commercially available 4-acetylbenzenesulfonyl chloride.

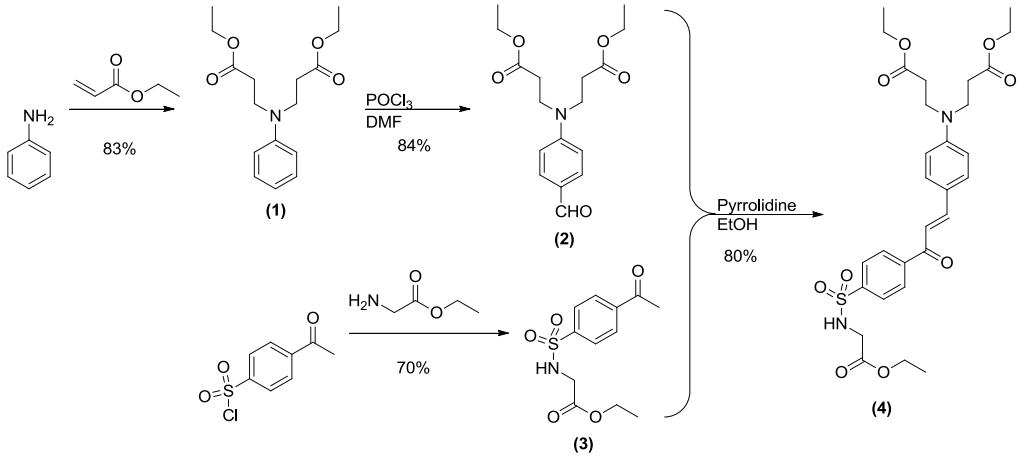

Scheme 2.1: Synthesis of chalcone **4**.

To construct the pyrazoline core, chalcone **4** was reacted with the corresponding protected arylhydrazine[1, 3a, b] (Scheme 2.2). Some cleavage of the acetonide moiety was observed, most likely due to the acidic reaction conditions. For this reason, the crude product was subjected to reaction with acetone diethylacetal to fully recover the partially deprotected product.

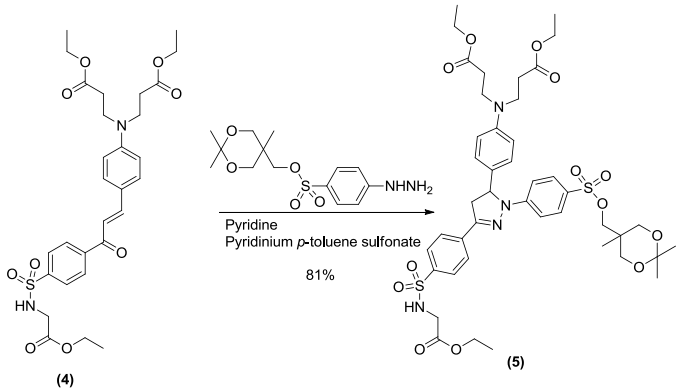

Scheme 2.2: Synthesis of the 1,3,5-triarylpyrazoline core.

For the synthesis of derivatives **6-8**, the fully protected pyrazoline **5** was alkylated at the sulfonamide nitrogen with a range of alkyl bromides of different chain lengths (Scheme 2.3a), followed by hydrolysis under acidic conditions to give the corresponding diol derivatives. It was anticipated that both hydrolysis of the ester groups as well as deprotection of the sulfonic acid would occur under strongly basic conditions, as the mono-deprotonted diol could undergo an intramolecular ring closure to form the corresponding oxetane and release the sulfonate moiety as illustarted with Scheme 2.3b. The first attempt to remove the neopentyl protective group and hydrolyze all esters with potassium hydroxide produced the final pyrazoline derivatives after 3 days. This long reaction time is presumably due to the rate limiting ring closure and formation of the oxetane.

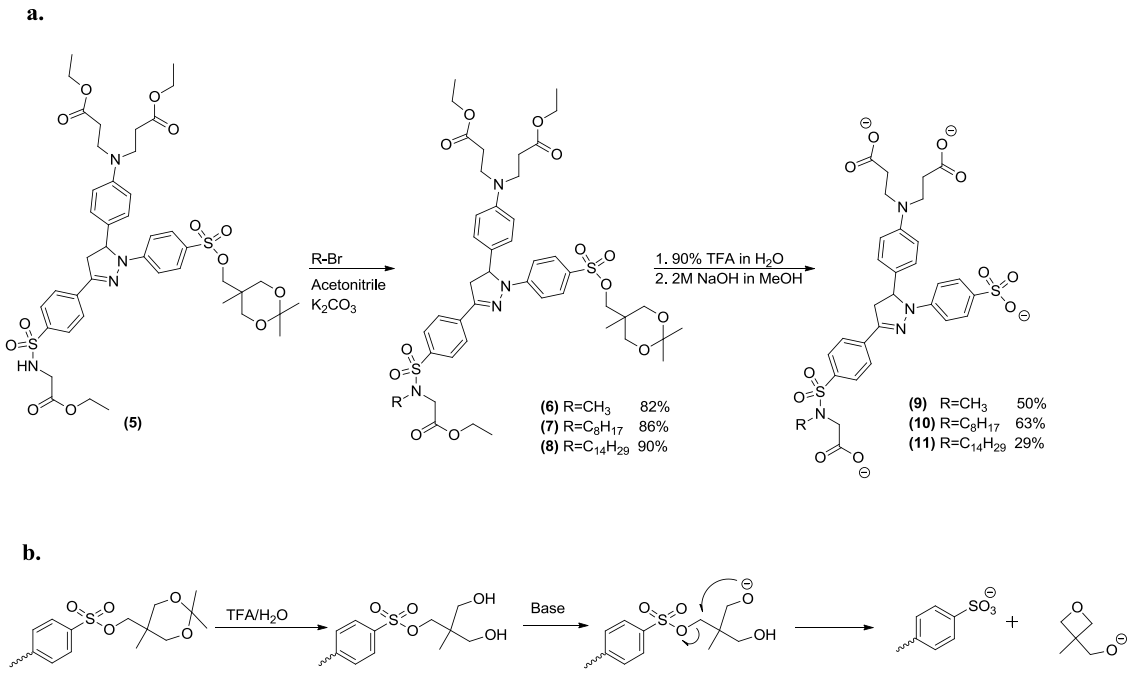

Scheme 2.3: Synthesis of 1,3,5-triarylpyrazoline derivatives **9-11.** a. Synthetic scheme. b. Proposed mechanism for removal of neopentyl protective group.

After HPLC purification of the final products, the ^{1}H-NMR spectra revealed unexpected impurities in the aromatic region (6 to 8ppm). It is well-known that pyrazolines are susceptible towards photo-oxidation to produce the corresponding pyrazoles as outlined in Figure 2.2. For example Rivett et al[4]. showed that irradiation of 1,3,5-triarylpyrazolines at wavelengths ranging between 370-380 nm led to 50% conversion of the pyrazolines to the corresponding photo-oxidized pyrazoles within an average of 90 minutes. The pyrazole formation was readily identified based on the characteristic singlet resonance near 7.0 ppm in the ^{1}H-NMR spectrum.[4]

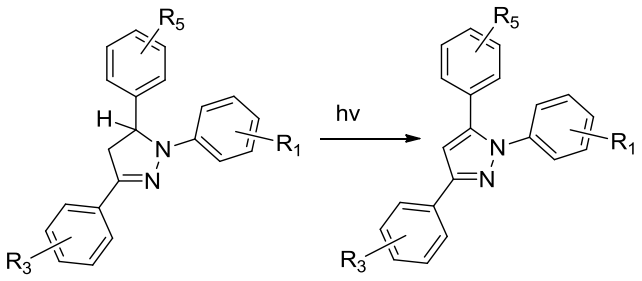

Figure 2.2: Photo-oxidation of 1,3,5-triarylpyrazolines to the corresponding pyrazoles.

To improve the overall yield and purity of the product, the reaction conditions were further optimized by limiting exposure to light and utilizing a stronger base to favor a faster deprotection. As previously reported, the neopentyl diol intermediate can be effectively removed by potassium *tert*-butoxide in tetrahydrofuran (THF),[3e] which is poorly solvated in this solvent and therefore much more basic compared to aqueous solutions. The reaction with potassium *tert*-butoxide in THF was indeed much faster compared to potassium hydroxide and after 15 minutes most of the starting material was converted to the sulfonate product. After hydrolysis of the esters and purification via HPLC, ^{1}H-NMR analysis showed that presumably intermediate **13** was formed rather than the desired product (as the ammonium salt). Because the sulfonamide moiety is separated by only one carbon from the electron withdrawing carboxyl group, the glycyl ester can undergo elimination through an E1cb type mechanism as proposed in Scheme 2.4.

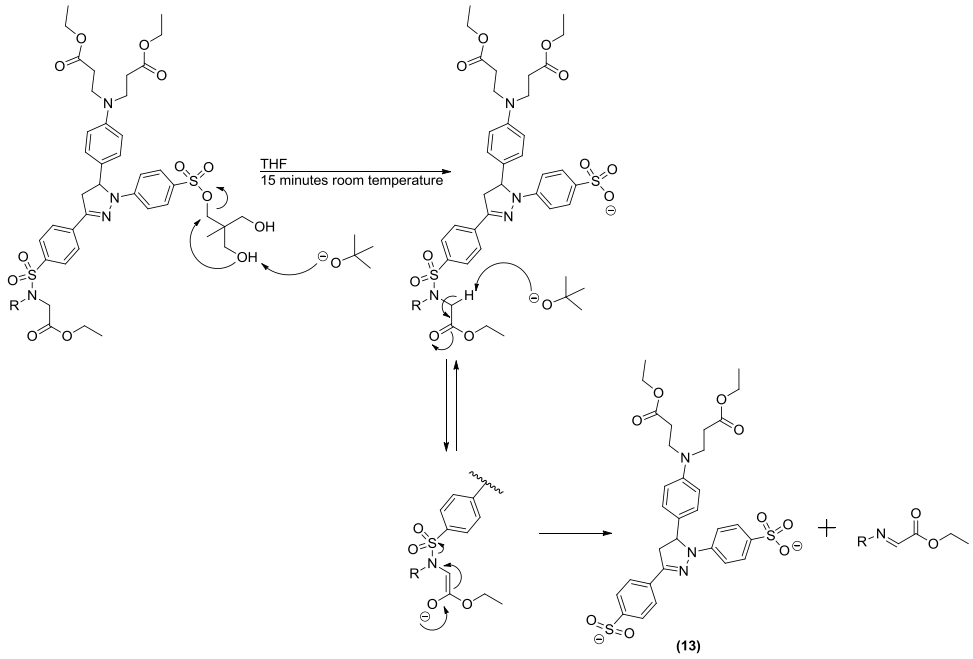

Scheme 2.4: Proposed mechanism for the cleavage of the carboxymethyl sulfonamide functionality.

Since secondary sulfonamides can be readily deprotonated[5] to render them less susceptible for the proposed cleavage mechanism, the protective groups were removed prior to alkylation of the sulfonamide; however, the latter conversion produced the desired product in only 0.5% yield, (Scheme 2.5). The low yield is most likely due to insufficient concentration of the reaction partners within the solvent system used for the conversion.

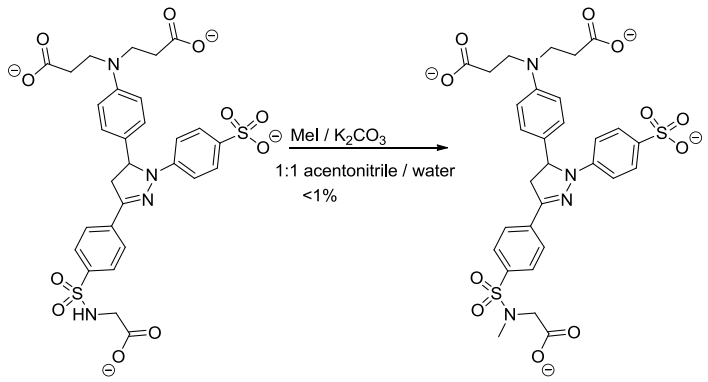

Scheme 2.5: Alkylation of the hydrolyzed pyrazoline intermediate under biphasic reaction conditions.

Based on these unsuccessful attempts, the initially used reaction conditions were re-evaluated. This time, the deprotection was carried out under strict exclusion of oxygen and protection from light, producing now the final desired products with 29% to 63% yield.

2.3 Photophysical characterization

To gauge the effect of membrane proximity on the PET process, the HPLC-purified 1,3,5-triarylpyrazolines **9-11** were first characterized in neat aqueous buffer solution (Table 2.1). For all derivatives, the absorption and emission maxima were determined in 10 mM MOPS buffer (pH 8.5). To determine the pK_a value of the aniline nitrogen, compound **9** was subjected to a spectrophotometric potentiometric titration in 0.1 M KCl as ionic background, yielding a value of 5.96 ± 0.02.

Table 2.1: Photophysical characterization of 1,3,5-triarlypyrazolines **9-11**

		λ (nm)			Φ_F[b]		
Compound[a]	**R**	**abs**	**em**	**pK_a**[c]	**Φ acid**[d]	**Φ base**[e]	**f_e**[f]
9	CH_3	382	504	5.96	0.2698	0.0013	207
10	C_8H_{17}	386	495			0.0011	
11	$C_{14}H_{29}$	389	492			0.0013	

[a]ammonium salt. [b] Fluorescence quantum yield (norharmane in 0.1 N H_2SO_4 as reference). [c]pK_a titration was done in 1 mM PIPES, 1 mM PIPBS 0.1M KCl (pH 8.5) as described in the material and methods section. [d]10mM MOPS/K^+, pH 4. [e]10 mM MOPS/K^+, pH 11. [f]fluorescence enhancement factor calculated as the ratio between the acid and basic quantum yields. abs = absorption, em = emission.

This pK_a value served as an important reference point to ensure that the quantum yields of the protonated and deprotonated forms (acquired at a pH 4 and 8.5, respectively) were only of a single species. Because compounds **10** and **11** were expected to have very similar pK_a values, the potentiometric titration was only carried out with compound **9**. Protonation of compound **9** induced a 207-fold increase in fluorescence. As shown in Table 2.1, all three compounds were found to have similar quantum yields under basic conditions at pH 11. Furthermore, the absorption and emission wavelengths were slightly affected by the alkyl chain lengths. While the absorption wavelength increased with increasing the alkyl chain length, the emission wavelength showed the opposite trend. It is noteworthy that the same effects on absorption and emission wavelengths were observed for the sulfonated pyrazoline derivative **CTAP-2** upon changing the solvent from water to octanol.

2.4 Cellular permeability

To test whether pyrazolines **9-11** might passively diffuse across the plasma membrane of mammalian cells, adherent NIH 3T3 cells were cultured in DMEM and incubated for 1 hour with 5 μM of each dye followed by fluorescence microscopy imaging. As shown in Figure 2.3, the cells are only weakly fluorescent compared to the background fluorescence of control cells that were not incubated with any compound, making it difficult to assess the degree of membrane permeability.

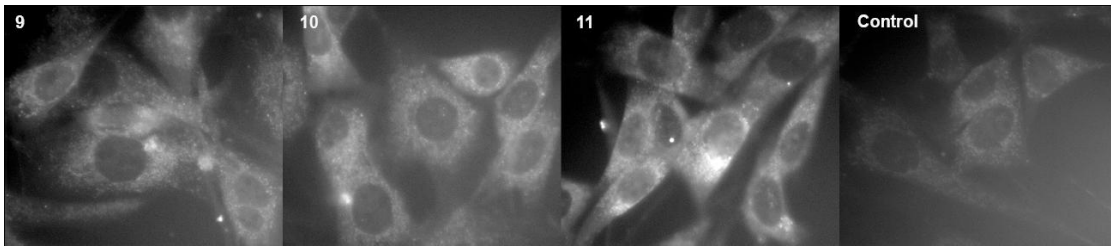

Figure 2.3: Fluorescent micrographs of NIH 3T3 cells incubated for an hour with 5 μM probe (final conc.) in DMEM at pH=7.2. Panel 9 represents cells incubated with compound **9**, panel 10 represents cells incubated with compound **10**, panel 11 represents cells incubated with compound **11** and panel control represents cells incubated with DMEM.

2.5 Material and methods

General: 4-Acetylbenzenesulfonylchloride (Fluka analytical), glycine ethylester hydrochloride (Sigma Aldrich), aniline (Alfa Aesar) and ethylacrylate (Acros organics), were commercially available. NMR: δ in ppm using $SiMe_4$ as a reference (0 ppm, 1H, 400 MHz). MS: selected peaks; *m/z*. Flash chromatography: Merck silica gel (70-230 mesh). TLC: 0.25 mm, Merck silica gel 60 F254, spots were visualized under 254 nm UV. Reversed phase HPLC was conducted with a 30 x 1 cm R-18 column at ambient temperature using an elution gradient of 0%-40% MeCN/0.1% aqueous NH_4HCO_3 over 80 minutes. The eluted products were freed of NH_4HCO_3 by repeated dissolution in methanol followed by evaporation under vacuum.

2.5.1 Synthesis of chalcone 4

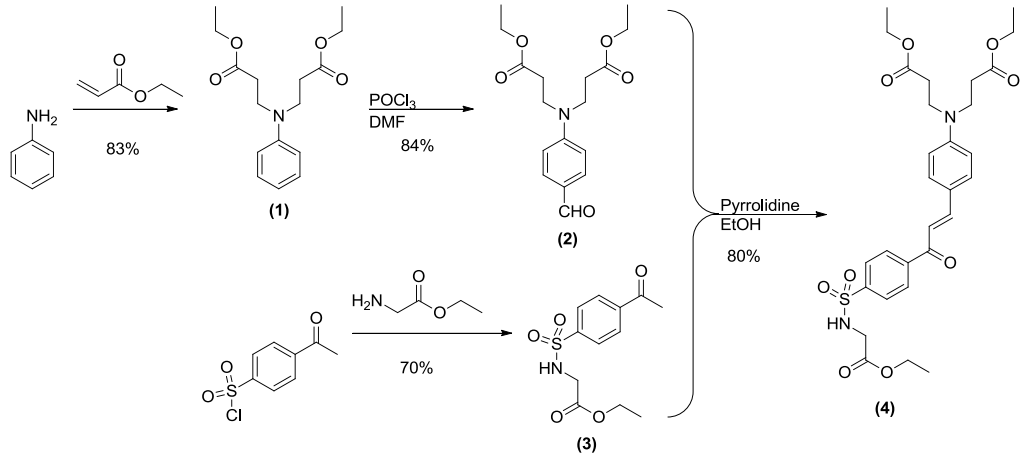

Scheme 2.6: Synthesis of intermediate **4**.

Ethyl 2-(4-acetylphenylsulfonamideo)acetate (1)

4-acetylbenzenesulfonylchloride (2.6 g, 0.019 mol) was dissolved in 6.0 mL of anhydrous pyridine and added slowly to a solution of glycine ethylester hydrochloride (3.44 g, 1.3 eq) in 4.0 mL of anhydrous pyridine. The combined mixture was stirred for 1 h under N_2 at room temperature. A color change, from yellow to red, was noticed over a period of 1 h. After addition of crushed ice the solution was diluted in H_2O (80 mL). The white crystalline product was filtered off and dried under vacuum. Yield: 2.77 g (51%). ^{1}H NMR ($CDCl_3$, 400 MHz) δ 1.19 (t, J = 7.12 Hz, 3H), 2.65 (s, 3H), 3.82 (d, J = 5.36 Hz, 2H), 4.10 (q, J = 7.15, 2H), 5.18 (t br, J = 5.27 Hz, 1H), 7.97 (dt, J = 8.64, 1.9 Hz, 2H), 8.10 (dt, J = 8.71, 1.9 Hz, 2H). ^{13}C NMR ($CDCl_3$, 400 MHz) δ 13.94, 26.83, 44.09, 62.01, 140.15, 143.25, 168.55, 196.70. EI HRMS *m/z* calculated for [M^+] $C_{12}H_{15}NO_5S$ 285.0671, found 285.0672.

Diethyl 3,3'-(phenylazanediyl)dipropanoate(2)

Freshly distilled aniline (4.08 g, 0.044 mol) was dissolved in 7.0 mL hexafluoro-2-propanol along with 14.0 mL ethylacrylate (13.16 g, 3 eq). Solution was stirred at 75 °C for 137 hours. Reaction was concentrated under vacuum. Product was purified by column chromatography (10:1 hexanes ethyl acetate) yielding a mixture of di-substituted and mono-substituted products (5:1), (83% di-substitution). ^{1}H NMR ($CDCl_3$, 400 MHz) δ 1.25 (t, J = 7.14 Hz, H), 2.58 (t br,J = 7.34, 7.24 Hz, 4H), 3.66 (t br, J = 7.34, 7.24 Hz, 4H), 4.14 (q, J = 7.15Hz, 4H), 6.70-6.74 (m, 3H), 7.22-7.26 (m, 2H). ^{13}C NMR ($CDCl_3$, 400 MHz) δ 14.18, 32.49, 46.85, 60.57, 112.58, 116.97, 129.45, 146.76, 172.09. EI HRMS *m/z* calculated for [M^+] $C_{16}H_{23}NO_4$ 293.1627, found 293.1630.

Diethyl 3,3'-((4-formylphenyl)azanediyl)dipropanoate (3)

Dimethylformamide (5.5 mL, 70.92 mmol) was cooled in an ice bath, and $POCl_3$ (3.5 mL, 35.5 mmol) was added drop wise. The resulting mixture was added to a solution of ethyl 2-(4-acetylphenylsulfonamideo) acetate (1.1516 g, 3.94 mmol) in DMF (1.0 mL). After stirring for 80 minutes at 75 °C the mixture was cooled to room temperature, poured into water (20 mL), and made basic with 35.5 mL of 20% NaOH. The mixture was extracted with methyl *tert*-butyl ether (MTBE, 2 x 20 mL). The combined organic extracts were dried over dried over Na_2SO_4 and concentrated under reduced pressure to give the product as yellow oil. Yield: 0.9282 g (73%). ^{1}H NMR ($CDCl_3$, 400 MHz) δ 1.26 (t, J = 7.18 Hz, 6H), 2.63 (t, J = 7.23 Hz, 4H), 3.77 (t, J = 7.29 Hz, 4H), 4.15 (q, J = 7.18, 4H), 6.73 (d, J = 9.12 Hz, 2H), 7.74 (d, J = 9.08 Hz, 2H), 9.75 (s, 1H). ^{13}C NMR

($CDCl_3$, 400 MHz) δ 14.10, 32.24, 45.60, 60.82, 111.20, 125.87, 132.18, 151.39, 171.41, 190.12. EI HRMS *m/z* calculated for [M^+] $C_{17}H_{23}NO_5$ 321.1576, found 321.1566.

(*E*)-diethyl 4-(4-(3-(4-(*N*-(2-ethoxy-2-oxoethyl)sulfamoyl)phenyl)-3-oxoprop-1-en-1-yl)phenyl)heptanedioate (4)

Aldehyde **3** (480 mg, 1.493 mmol) and ethyl 2-(4-acetylphenylsulfonamideo)acetate (212 mg, 0.746 mmol 0.5 equiv) were dissolved in 2.97 mL of ethanol. Pyrrolidine (184 µL, 1.5 equiv) was then added, the reaction flask was sealed and the mixture was stirred for 3 hours. The mixture was diluted with 10.0 mL H_2O and 1.0 M mono sodium phosphate (2.0 mL) and extracted with ethyl acetate (2 x 20 mL). The combined organic extracts were dried over Na_2SO_4 concentrated under reduced pressure to give crude dark red oil. Product was purified by column chromatography (1:1 hexanes ethyl acetate) to give orange oil. Yield 382 mg (87%), aldehyde **2** was recovered in the same conditions (66%). ^{1}H NMR ($CDCl_3$, 400 MHz) δ 1.19 (t, *J* = 7.13 Hz, 3H), 1.26 (t, *J* = 7.16 Hz, 6H), 2.62 (t, *J* = 7.19 Hz, 4H), 3.75 (t, *J* = 7.25 Hz, 4H), 3.82 (d, *J* = 5.41 Hz, 2H), 4.10 (q, *J* = 7.02 Hz, 2H), 4.16 (q, *J* = 7.02 Hz, 4H), 5.15 (t, *J* = 5.39 Hz, 1H), 6.715 (d, *J* = 9.41 Hz, 2H), 7.26 (d, *J* = 15.66 Hz, 1H), 7.55 (d, *J* = 9.21 Hz, 2H), 7.78 (d, *J* = 15.66 Hz, 1H), 7.98 (d, *J* = 8.65 Hz, 2H), 8.08 (d, *J* = 8.65 Hz, 2H). ^{13}C NMR ($CDCl_3$, 400 MHz) δ 13.99, 14.17, 32.38, 44.16, 46.63, 60.85, 62.02, 111.98, 116.63, 122.85, 127.36, 128.90, 131.06, 142.14, 142.64, 147.04, 149.18, 168.63, 171.65, 189.34. EI HRMS *m/z* calculated for [M^+]$C_{30}H_{37}N_2O_9S$ 588.2142, found 588.2131.

2.5.2 Synthesis of alkylated protected pyrazoline derivatives 6-8

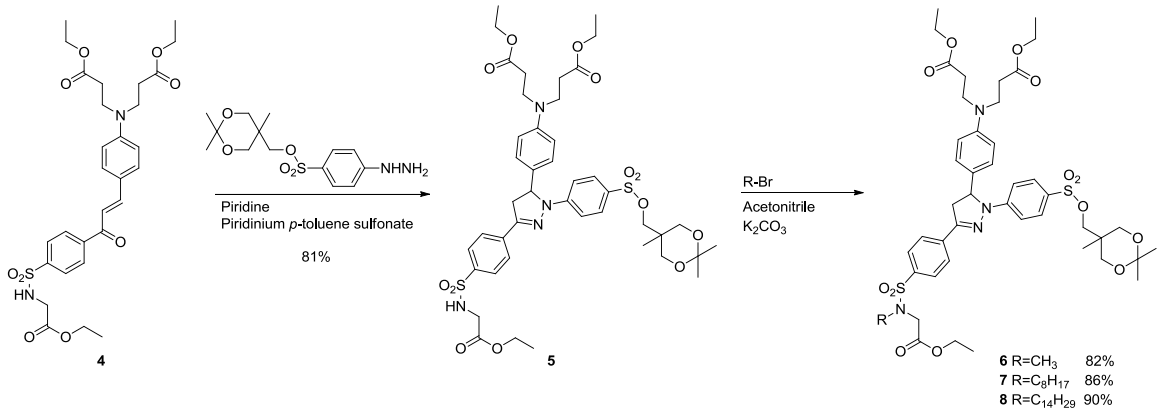

Scheme 2.7: Synthesis of pyrazoline intermediates **6-8**.

Diethyl 3,3'-((4-(3-(4-(*N*-(2-ethoxy-2-oxoethyl)sulfamoyl)phenyl)-1-(4-(((2,2,5-trimethyl-1,3-dioxan-5-yl)methoxy)sulfonyl)phenyl)-4,5-dihydro-1*H*-pyrazol-5-yl)phenyl)azanediyl)dipropanoate (5)

A mixture of chalcone **4**, (682 mg, 1.15 mmol), (2,2,5-trimethyl-1,3-dioxan-5-yl)methyl 4-hydrazinylbenzenesulfonate (575 mg, 1.72 mmol) and pyridinium *p*-toluene sulfonate (291 mg, 1.15 mmol) in 2.0 mL pyridine was stirred in a sealed flask under N_2 at 93 °C for 30 hours. After cooling to room temperature, the reaction mixture was diluted in 10 mL dichloromethane followed by 10 mL xylenes and concentrated under reduced pressure. The residue was taken up in acetone (20 mL). Acetone diethylacetal (7.0 mL) was added followed by *p*-toluenesulfonic acid monohydrate (800 mg, 4 equiv.), and the mixture was stirred for 1 hour at room temperature. It was then made basic with 20% aqueous ammonia (1 mL), poured into water (140 mL) with brine (5 mL), and extracted with dichloromethane (3 x 35 mL). The combined extracts were dried with Na_2SO_4, concentrated under reduced pressure, and subjected to sequential column chromatography with hexanes-ethyl acetate (1:1) followed by pure dichloromethane to give the product as

a yellow glassy solid. Yield 848 mg (0.941 mmol, 81.8%).^{1}H NMR ($CDCl_3$, 400 MHz) δ 0.82 (s, 3H), 1.18-1.25 (m, 12H), 1.37 (s, 3H), 2.55 (t, *J* = 7.31 Hz, 4H), 3.18 (dd, *J* = 17.11, 5.7 Hz, 1H), 3.55, (s, 4H), 3.63 (t br, *J* = 7.21 Hz, 4H), 3.81 (d, *J* = 5.50 Hz, 2H), 3.85 (dd, *J* = 5.39 , 1H), 4.04 (s, 2H), 4.08-4.14 (m, 6H), 5.12 (t, *J* = 5.41), 5.35 (dd, *J* = 6.22, 5.68 Hz, 1H), 6.64 (d, *J* = 9.06 Hz, 2H), 7.07 (d, *J* = 9.06 Hz, 2H), 7.17 (d, *J* = 9.06 Hz, 2H), 7.70 (d, *J* = 9.26 Hz, 2H), 7.84 (dd, *J*=8.72, 2H), 7.89 (dd, *J* = 8.79, 2H).^{13}C NMR ($CDCl_3$, 400 MHz) δ 13.94, 14.09, 17.21, 19.49, 27.43, 32.33, 33.81, 44.07, 46.61, 60.56, 61.91, 63.40, 65.58, 65.64, 72.06, 97.94, 112.75, 112.91, 124.13, 126.34, 126.73, 127.51, 128.22, 129.50, 136.44, 138.99, 146.56, 147.43, 147.74, 168.62, 171.81. EI HRMS *m/z* calculated for [M^+] $C_{43}H_{56}N_4O_{13}S_2$ 900.3285, found 900.3214.

Diethyl 3,3'-((4-(3-(4-(*N*-(2-ethoxy-2-oxoethyl)-*N*-methylsulfamoyl)phenyl)-1-(4-(((2,2,5-trimethyl-1,3-dioxan-5-yl)methoxy)sulfonyl)phenyl)-4,5-dihydro-1*H*-pyrazol-5-yl)phenyl)azanediyl)dipropanoate (6)

A mixture of Pyrazoline 5 (200 mg, 0.222 mmol), iodomethane (35 µL, 0.555 mmol) and potassium carbonate (61.5 mg, 0.444 mmol) in 1.0 mL anhydrous acetonitrile was stirred in a sealed flask under N_2 room temperature for 4 hours. Potassium carbonate (92 mg, 0.666 mmol) and iodomethane (35 µL, 0.555 mmol) were added and reaction was stirred under the same conditions for an additional hour. The reaction mixture was diluted with 20 mL of ethyl-acetate and washed with water (3 x 10 mL). The organic layer was dried over Na_2SO_4 concentrated under reduced pressure and subjected to sequential column chromatography with dichloromethane methyl *tert*-butyl ether (20:1) to give product as a yellow glassy solid. Yield 167 mg (0.182 mmol, 82%). ^{1}H NMR ($CDCl_3$, 400 MHz) δ

0.82 (s, 3H), 1.21-1.25 (m, 12H), 1.37 (s, 3H), 2.55 (t, *J* = 7.37, 7.03 Hz, 4H), 2.92 (s, 3H), 3.19 (dd, *J* = 17.51, 5.79, 1H), 3.56 (s, 4H), 3.63 (t, *J* = 7.48, 7.00 Hz, 4H), 3.86 (dd, *J* = 17.51, 12.22 Hz, 1H), 4.02 (S, 4H), 4.04 (s, 2H), 4.09-4.16 (m, 6H), 5.35 (dd, *J* = 12.10, 5.66, 1H), 6.65 (d, *J* = 8.87 Hz, 2H), 7.08 (d, *J* = 8.80 Hz, 2H), 7.17 (d, *J* = 8.92 Hz, 2H), 7.70 (d, *J* = 9.16 Hz, 2H), 7.85 (s, 4H). ^{13}C NMR ($CDCl_3$, 400 MHz) δ 14.08, 14.16, 17.28, 19.56, 27.45, 32.40, 33.88, 35.62, 43.32, 46.68, 51.00, 60.65, 61.42, 63.43, 65.64, 65.70, 72.20, 98.00, 112.81, 112.94, 124.11, 126.28, 126.81, 127.76, 128.33, 129.57, 136.28, 138.27, 146.62, 147.53, 147.91, 168.35, 171.88. EI HRMS *m/z* calculated for [M^+] $C_{44}H_{58}N_4O_{13}S_2$ 914.3442, found 914.3398.

Diethyl 3,3'-((4-(3-(4-(*N*-(2-ethoxy-2-oxoethyl)-*N*-octylsulfamoyl)phenyl)-1-(4-(((2,2,5-trimethyl-1,3-dioxan-5-yl)methoxy)sulfonyl)phenyl)-4,5-dihydro-1*H*-pyrazol-5-yl)phenyl)azanediyl)dipropanoate (7)

A mixture of pyrazoline **5** (100 mg, 0.111 mmol), 1-bromooctane (30 µL, 0.173 mmol) and potassium carbonate (31 mg, 0.224 mmol) in 1.0 mL anhydrous acetonitrile was stirred in a sealed flask under N_2 at 60 °C for 12 hours. After cooling to room temperature, the reaction mixture was diluted with 10 mL water and extracted with ethyl-acetate. The organic layer was dried with Na_2SO_4, concentrated under reduced pressure, and subjected to sequential column chromatography with dichloromethane, hexanes and methyl *tert*-butyl ether (3:3:1). Yield 80 mg (0.079 mmol, 71%). ^{1}H NMR ($CDCl_3$, 400 MHz) δ 0.81 (s, 3H), 0.86 (t, *J* = 7.12, 6.75, 3H), 1.20-1.25 (m, 24H), 1.37 (s, 3H), 1.53 (t br, *J* = 6.84, 5.91, 2H), 2.55 (t, *J* = 7.35, 7.07 Hz, 4H), 3.16-3.26 (m, 3H), 3.55 (s, 4H), 3.63 (t, *J* = 7.33, 6.95 Hz, 4H), 3.85 (dd, *J* = 16.88, 12.22 Hz, 1H), 4.03 (s, 2H), 4.08-

4.14 (m, 8H), 5.34 (dd, *J* = 12.53, 5.88 Hz, 1H), 6.65 (d, *J* = 8.84 Hz, 2H), 7.08 (d,*J* = 8.84 Hz, 2H), 7.16 (d, *J* = 9.00 Hz, 2H), 7.70 (d, *J* = 9.18, 2H), 7.81-7.88 (m, 4H).^{13}C NMR ($CDCl_3$, 400 MHz) δ 14.07, 14.16, 17.28, 19.57, 22.60, 26.52, 27.48, 27.80, 29.10, 29.12, 31.71, 32.40, 33.87, 43.34, 46.68, 47.81, 48.25, 60.64, 61.34, 63.40, 65.65, 65.70, 72.10, 98.00, 112.81, 112.92, 124.03, 126.17, 126.81, 127.73, 128.37, 129.562, 136.056, 139.82, 146.60, 147.57, 148.03, 168.88, 171.87. EI HRMS *m/z* calculated for [M^+] $C_{51}H_{72}N_4O_{13}S_2$ 1012.4537, found 1012.4512.

Diethyl 3,3'-((4-(3-(4-(*N*-(2-ethoxy-2-oxoethyl)-*N*-tetradecylsulfamoyl)phenyl)-1-(4-(((2,2,5-trimethyl-1,3-dioxan-5-yl)methoxy)sulfonyl)phenyl)-4,5-dihydro-1*H*-pyrazol-5-yl)phenyl)azanediyl)dipropanoate (8)

A mixture of pyrazoline **5** (100 mg, 0.111 mmol), 1-bromotetradecane (50 µL, 0.166 mmol) and potassium carbonate (38.5 mg, 0.277 mmol) in 1.0 mL anhydrous acetonitrile was stirred in a sealed flask under N_2 at 60 °C for 12 hours. 66 µL of 1-bromotetradecane was added and reaction was stirred under the same conditions for 15 minutes. After cooling to room temperature, the reaction mixture was diluted with 10 mL water and extracted with ethyl-acetate. The organic layer was dried with Na_2SO_4, concentrated under reduced pressure, and subjected to sequential column chromatography with dichloromethane, hexanes and methyl *tert*-butyl ether (3:3:1). Yield 99.8 mg (0.091 mmol, 82%). ^{1}H NMR ($CDCl_3$, 400 MHz) δ 0.81 (s, 3H), 0.88 (t, *J* = 7.03 Hz, 3H), 1.20-1.25 (m, 34H), 1.37 (s, 3H), 1.53 (t Br, 2H), 2.55 (t, *J* = 7.25, 7.09 Hz, 4H), 3.16-3.26 (m, 3H), 3.55 (s, 4H), 3.63 (t, *J* = 7.25, 7.09 Hz, 4H), 3.85 (dd, *J* = 17.66, 12.26 Hz, 1H), 4.04 (s, 2H), 4.08-4.14 (m, 8H), 5.34 (dd, *J* = 12.26, 5.61 Hz, 1H), 6.64 (d, *J* = 8.68 Hz, 2H),

7.08 (d, *J* = 8.56 Hz, 2H) 7.16 (d, *J* = 8.79 Hz, 2H), 7.69 (d, *J* = 8.88 Hz, 2H), 7.82-7.88 (m, 4H). ^{13}C NMR ($CDCl_3$, 400 MHz) δ 14.07, 14.11, 14.16, 17.27, 19.57, 22.63, 22.66, 26.54, 27.47, 27.83, 29.17, 29.33, 29.48, 29.52, 29.61, 29.62, 29.66, 31.56, 31.89, 32.40, 33.87, 43.34, 46.68, 47.81, 48.25, 60.63, 61.33, 63.41, 65.65, 65.70, 72.09, 97.99, 112.82, 112.92, 124.05, 126.17, 126.81, 127.72, 128.38, 129.55, 136.05, 139.82, 146.61, 147.56, 148.00, 168.86, 171.85. EI HRMS *m/z* calculated for [M^+] $C_{57}H_{84}N_4O_{13}S_2$ 1096.5476, found 1096.5451.

2.5.3 Hydrolysis of protective groups for the formation of derivatives 9-11

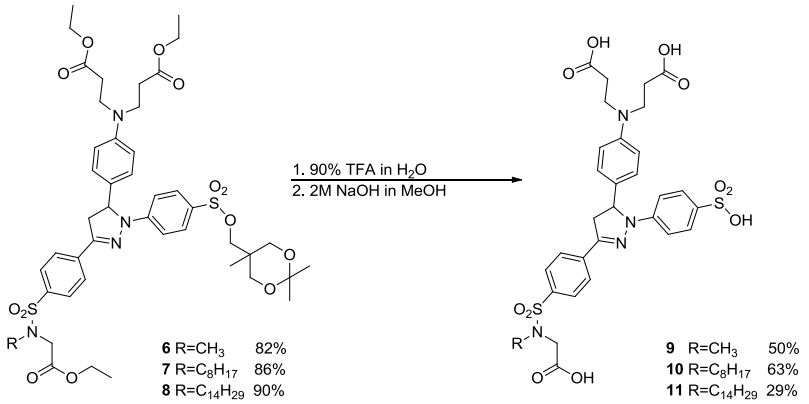

Scheme 2.8: Synthesis of pyrazoline derivatives **9-11**.

3,3'-((4-(3-(4-(*N*-(carboxymethyl)-*N*-methylsulfamoyl)phenyl)-1-(4-sulfophenyl)-4,5-dihydro-1*H*-pyrazol-5-yl)phenyl)azanediyl)dipropanoic acid (9)

Pyrazoline **6** (50 mg, 0.0546 mmol) was dissolved in a mixture of 90% trifluoroacetic acid and 10% H_2O (w/w, 2.7 mL) and stirred for 12 minutes at room temperature after complete dissolution. The reaction mixture was diluted with H_2O (5 mL), stirred for an additional 15 minutes, poured into H_2O (25 mL), rinsed completely with ethanol (10 mL),

cooled by adding crushed ice, and made basic with 28% aqueous ammonia (15mL). The resulting suspension was stirred for 30 minutes at 0 °C and the intermediate was then collected by extraction with ethyl-acetate, dried with Na_2SO_4 and concentrated under reduced pressure to give yellow oil. The mixture was dissolved in 1.0 mL methanol, NaOH was added (122.54 mg, 3.06 mmol to give a concentration of 2M) and the reaction was stirred at room temperature under N_2 in the dark for 18 hours. The reaction was quenched with acetic acid (175 µL, 3.057 mmol) and was subjected for HPLC purification (0-40% acetonitrile gradient in 0.1% ammonium bicarbonate H_2O over 80 minutes). Yield 20.5 mg (0.027 mmol, 50%). Product was isolated as the ammonium salt. ^{1}H NMR ($CDCl_3$, 400 MHz) δ 2.47 (t, J = 7.45, 7.06 Hz, 4H), 2.81 (s, 3H), 3.13 (dd, J = 17.72, 6.08 Hz, 1H), 3.59-3.64 (m, 6H), 3.87 (dd, J = 17.00, 12.32 Hz, 1H), 5.42 (dd, J = 12.22, 6.05 Hz, 1H), 6.71 (d, J = 8.79 Hz, 2H), 7.09 (d, J = 8.76 Hz, 2H), 7.12 (d, J = 9.04 Hz, 2H), 7.61 (d, J = 9.02 Hz, 2H), 7.82 (d, J = 8.79, 2H), 7.93 (d, J = 8.69, 2H). ^{13}C NMR ($CDCl_3$, 400 MHz) δ 32.50, 34.91, 42.56, 46.89, 48.43, 63.67, 112.45, 112.70, 125.82, 126.48, 126.66, 127.46, 129.42, 135.02, 136.92, 136.98, 145.44, 146.56, 146.64, 173.11, 175.34. EI HRMS *m/z* calculated for [M+H$^+$] $C_{31}H_{33}N_4O_{11}S_2$ 689.1676, found 689.1587.

3,3'-((4-(3-(4-(*N*-(carboxymethyl)-N-octylsulfamoyl)phenyl)-1-(4-sulfophenyl)-4,5-dihydro-1*H*-pyrazol-5-yl)phenyl)azanediyl)dipropanoic acid (10)

Pyrazoline **7** (145 mg, 0.143 mmol) was dissolved in a mixture of 90% trifluoroacetic acid and 10% H_2O (w/w, 5.28 mL) and stirred for 12 minutes at room temperature after complete dissolution. The reaction mixture was diluted with H_2O (5 mL), stirred for an

additional 15 minutes, poured into H_2O (25 mL), rinsed completely with ethanol (10 mL), cooled by adding crushed ice, and made basic with 28% aqueous ammonia (7.16 mL). The resulting suspension was stirred for 30 minutes at 0 °C and the intermediate was then collected by extraction with ethyl-acetate, dried with Na_2SO_4 and concentrated under reduced pressure to give yellow oil. The mixture was dissolved in 4.0 mL methanol, NaOH was added (320 mg, 8 mmol, to give a concentration of 2M) and the reaction was stirred at room temperature under N_2 in the dark for 18 hours. The reaction was quenched with acetic acid (495 µL, 8.64 mmol) and was subjected for HPLC purification (0-40% acetonitrile gradient in 0.1% ammonium bicarbonate H_2O over 80 minutes). Yield 42 mg (0.049 mmol, 62.7% after recovery of starting material). Product was isolated as the ammonium salt. ^{1}H NMR ($CDCl_3$, 400 MHz) δ 0.85 (t, J = 7.15, 6.89 Hz, 3H), 1.15-1.29 (m, 10H), 1.43-1.50 (m, 2H), 2.46 (t, J = 7.21 Hz, 4H), 3.10 (dd, J = 17.64, 6.07 Hz, 1H), 3.27 (t, J = 7.70, 7.54 Hz, 2H), 3.61 (t, J = 7.33, 7.00 Hz, 4H), 3.81-3.88 (m, 3H), 5.39 (dd, J = 12.33, 5.94 Hz, 1H), 6.71 (d, J = 8.68 Hz, 2H), 7.07 (d, J = 8.57 Hz, 2H), 7.11 (d, J = 8.98 Hz, 2H), 7.61 (d, J = 8.94 Hz, 2H), 7.84-7.90 (m, 4H). ^{13}C NMR ($CDCl_3$, 400 MHz) δ 13.08, 20.28, 22.30, 26.40, 27.10, 28.85, 28.88, 31.51, 33.15, 42.61, 46.97, 47.13, 47.18, 47.40, 42.61, 47.13, 47.90, 48.10, 48.46, 63.60, 112.44, 112.55, 125.74, 126.47, 126.64, 127.30, 129.18, 134.84, 136.61, 139.62, 145.47, 146.64, 146.68, 174.01, 176.27. EI HRMS *m/z* calculated for [M^+] $C_{37}H_{47}N_4O_{11}S_2$ 787.2786, found 787.2683.

3,3'-((4-(3-(4-(*N*-(carboxymethyl)-*N*-tetradecylsulfamoyl)phenyl)-1-(4-sulfophenyl)-4,5-dihydro-1H-pyrazol-5-yl)phenyl)azanediyl)dipropanoic acid (11)

Pyrazoline **8** (166 mg, 0.151 mmol) was dissolved in a mixture of 90% trifluoroacetic acid and 10% H_2O (w/w, 5.28 mL) and stirred for 12 minutes at room temperature after complete dissolution. The reaction mixture was diluted with H_2O (5 mL), stirred for an additional 15 minutes, poured into H_2O (25 mL), rinsed completely with ethanol (10 mL), cooled by adding crushed ice, and made basic with 28% aqueous ammonia (7.16 mL). The resulting suspension was stirred for 30 minutes at 0 °C and the intermediate was then collected by extraction with ethyl-acetate, dried with Na_2SO_4 and concentrated under reduced pressure to give yellow oil. The mixture was dissolved in 4.0 mL methanol, NaOH was added (320 mg, 8 mmol, to give a concentration of 2M) and the reaction was stirred at room temperature under N_2 in the dark for 18 hours. The reaction was quenched with acetic acid (495 µL, 8.64 mmol) and was subjected for HPLC purification (20-40% acetonitrile gradient over in 0.1% ammonium bicarbonate H_2O over 20 minutes and then 40-70% over 12 minutes). Yield 36.6mg (0.038 mmol, 28.6% after recovery of starting material). Product was isolated as the ammonium salt. ^{1}H NMR ($CDCl_3$, 400 MHz) δ 0.89 (t, J = 7.02, 6.74 Hz, 3H), 1.21-1.25 (m, 22H), 1.48 (t br, J = 6.97, 6.87 Hz, 2H), 2.48 (t, J = 7.37, 7.17 Hz, 4H), 3.11 (dd, J = 17.60, 6.05 Hz, 1H), 3.27 (t, J = 7.73, 7.58 Hz, 2H), 3.61 (t, J = 7.32, 7.02 Hz, 4H), 3.82-3.89 (m, 3H), 5.40 (dd, J = 12.41, 6.00 Hz, 1H), 6.70 (d, J = 8.75 Hz, 2H), 7.08 (d, J = 8.79 Hz, 2H), 7.11 (d, J = 8.93 Hz, 2H), 7.61 (d, J = 8.90 Hz, 2H), 7.84-7.90 (m, 4H). ^{13}C NMR ($CDCl_3$, 400 MHz) δ 13.07, 22.33, 26.37, 27.13, 28.86, 29.06, 29.19, 29.24, 29.35, 29.39, 31.66, 32.85, 42.62, 47.02, 47.67, 47.88, 48.07, 48.44, 63.63, 112.43, 112.58, 125.72, 126.48, 126.65, 127.31, 129.27, 134.90, 136.63, 139.60, 145.45, 146.60, 146.65, 173.77, 175.80. EI HRMS *m/z* calculated for [M^+] $C_{43}H_{59}N_4O_{11}S_2$ 871.3674, found 871.3622.

2.5.4 pK_a measurements and Quantum yield determination

pK_a measurements: Fluorescence spectra and UV-vis absorption spectra were acquired in 0.1 M KCl as ionic background in 1 mM PIPES, 1 mM PIPBS (pH 8.5). The excitation wavelength was set at 380 nm and the emission scan ranged from 390–700 nm and 250-500 nm respectively. All solutions were filtered through 0.2 µm membrane filters to remove interfering dust particles or fibers. Three independent pK_a titrations were carried out at 7.06 µM concentration of compound **9** by adding HCl such that pH interval is 0.24 at each step. The data were analyzed by non-linear least-squares fitting using the Specfit software package[6]. pH ranges between 8.5 to 4.18.

Quantum Yields and Fluorescence Enhancement Factors: Quantum yield of compound **9** and fluorescence enhancement factor was determined in 0.1 M KCl, 10 mM MOPS buffer (pH 7.2), which had been filtered through a 0.45 µM membrane filter to remove dust particles. For quantum yield determination, excitation was at 380 nm and four data points with absorbances between 0.1 and 0.5 (l = 10 cm) were used. Norharmane was used as a standard with a known quantum yield of 58% in 0.1 M H_2SO_4. Equation 4.1 was used for a one point quantum yield determination in the case of liposome studies.

$$\Phi_x = \Phi_s \left(\frac{A_x}{A_s}\right)\left(\frac{I_x}{I_s}\right)\left(\frac{n_x}{n_s}\right)^2 \qquad (4.1)$$

Where Φ_x is the quantum yield of the unknown, Φ_s is the quantum yield of the standard, A_x is the optical density of the unknown, A_s is the optical density of the standard, I_x is the fluorescence intensity of the unknown, I_s is the fluorescence intensity of the standard and

n_x is the refractive index of the medium of the unknown and n_s is the refractive index of the medium of the standard.

APPENDIX A

^{1}H AND ^{13}C NMR SPECTRA

Ethyl 2-(4-acetylphenylsulfonamideo)acetate (1)

^{1}H NMR ($CDCl_3$, 400 MHz)

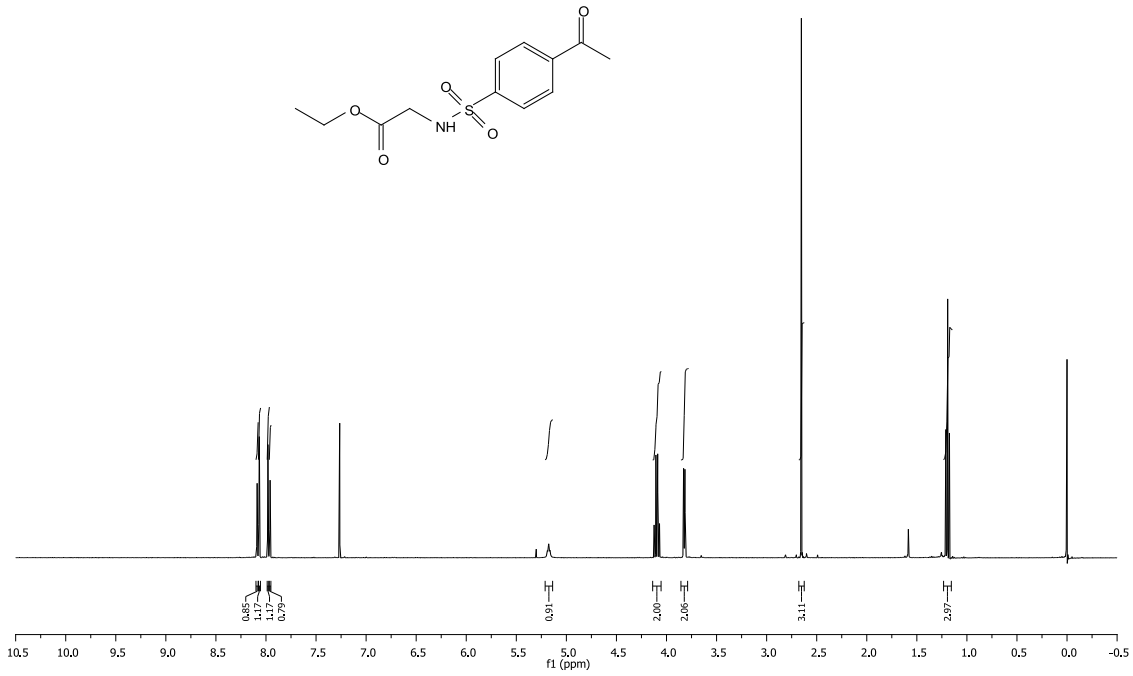

^{13}C NMR ($CDCl_3$, 400 MHz)

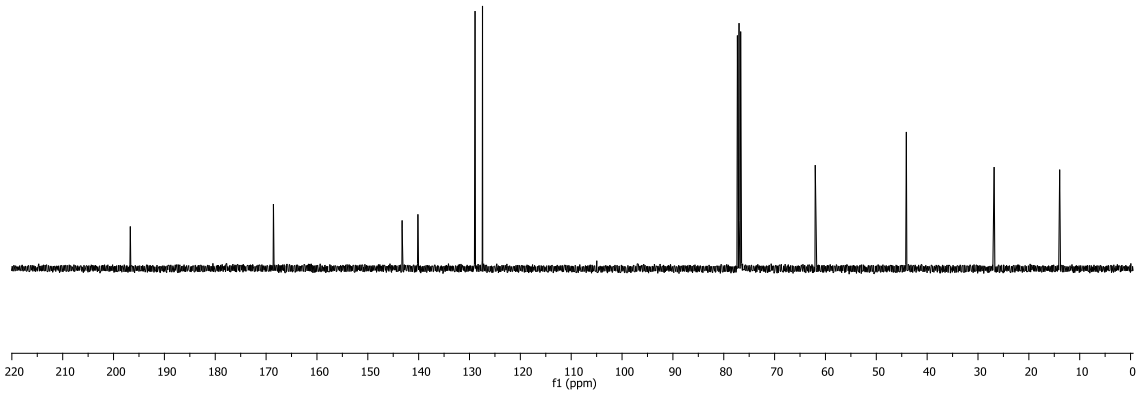

Diethyl 3,3'-(phenylazanediyl)dipropanoate(2):

^{1}H NMR ($CDCl_3$, 400 MHz)

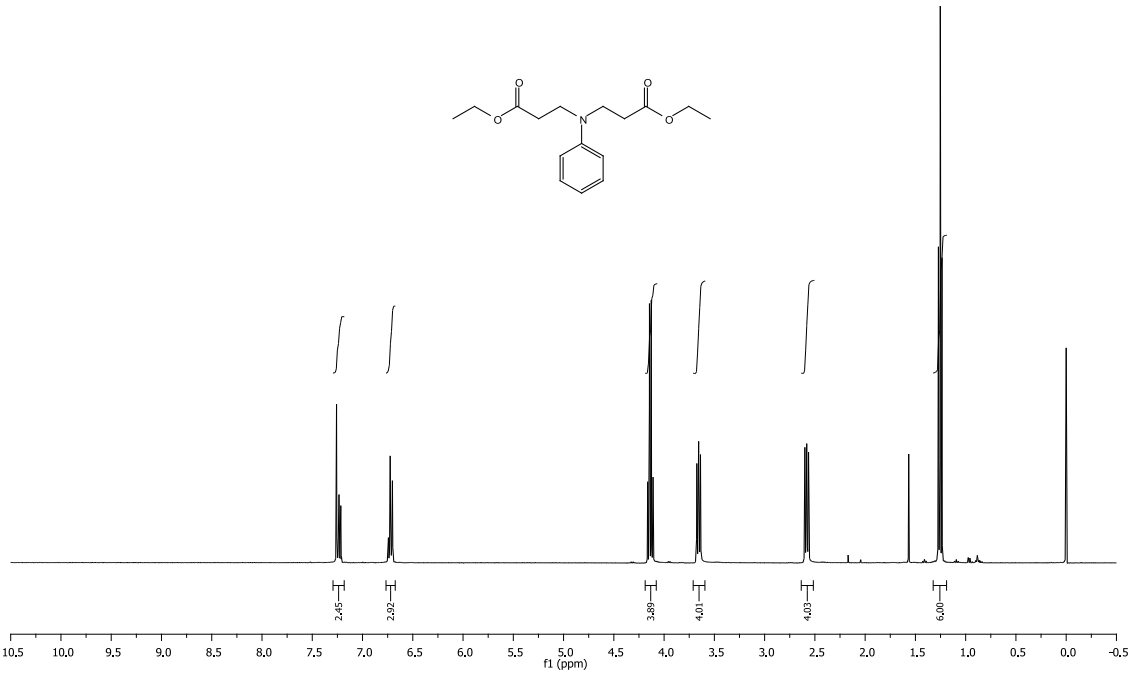

^{13}C NMR ($CDCl_3$, 400 MHz)

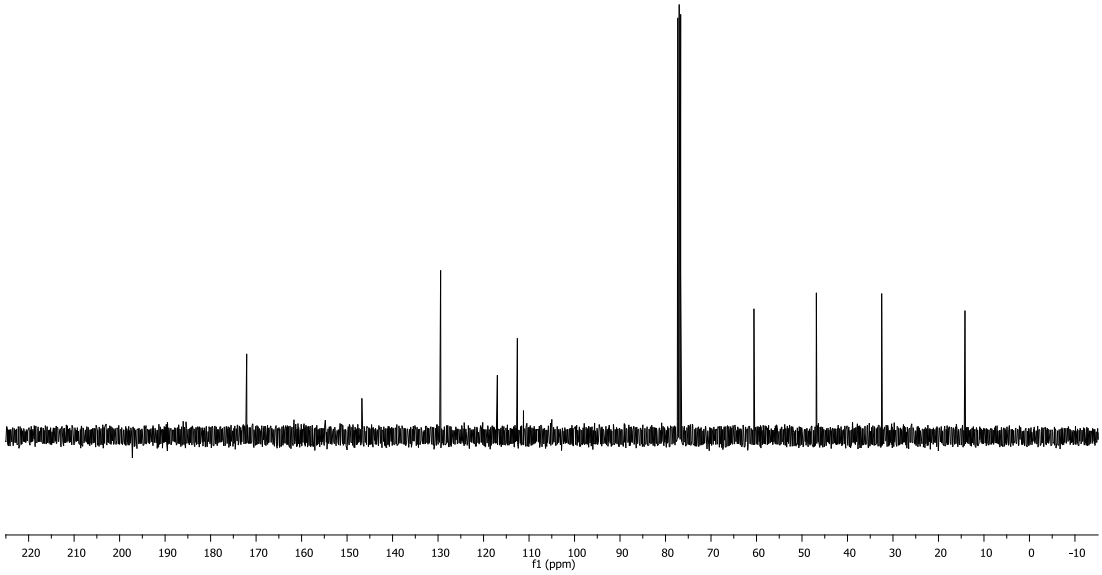

Diehtyl 3,3'-((4-formylphenyl)azanediyl)dipropanoate (3)

^{1}H NMR ($CDCl_3$, 400 MHz)

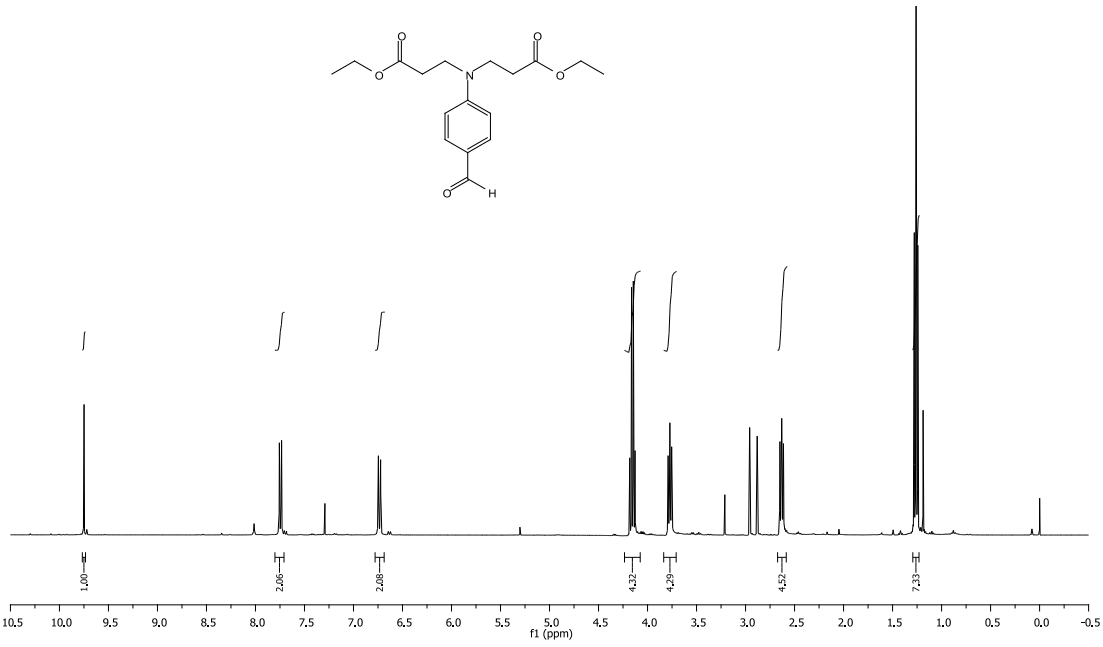

^{13}C NMR ($CDCl_3$, 400 MHz)

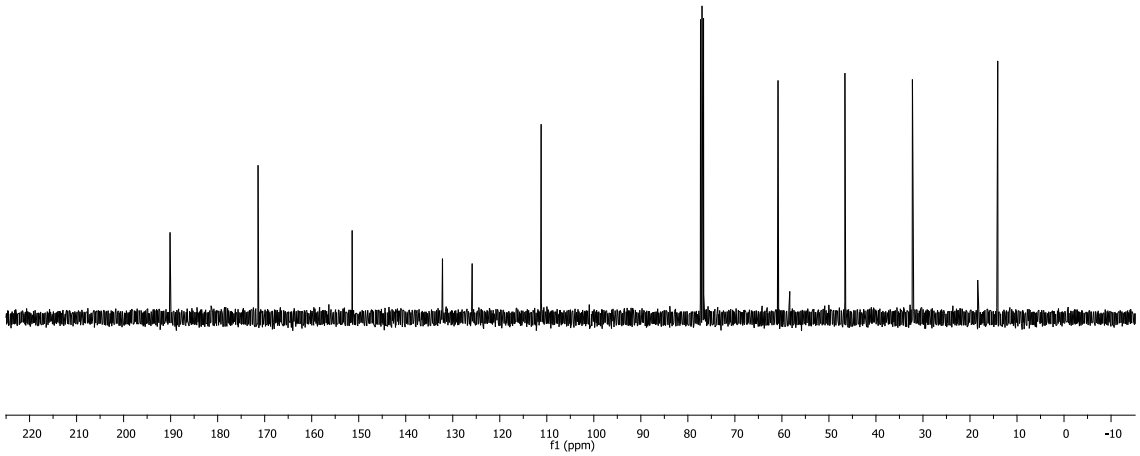

(*E*)-diethyl 4-(4-(3-(4-(N-(2-ethoxy-2-oxoethyl)sulfamoyl)phenyl)-3-oxoprop-1-en-1-yl)phenyl)heptanedioate (4)

^{1}H NMR ($CDCl_3$, 400 MHz)

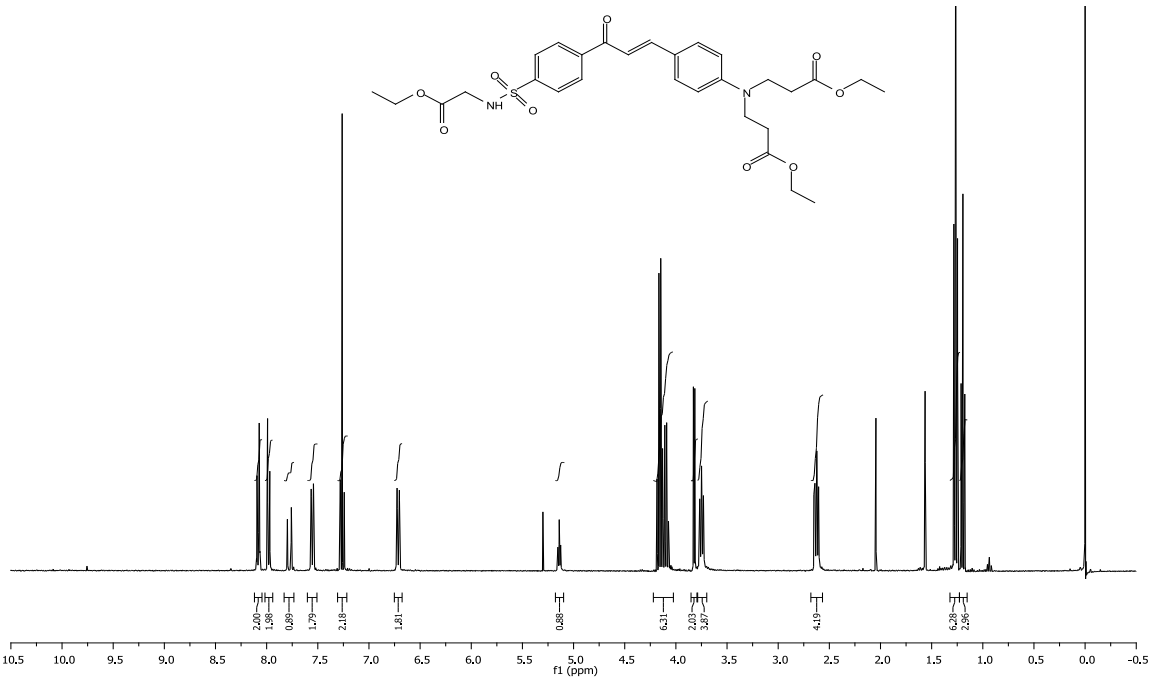

^{13}C NMR ($CDCl_3$, 400 MHz)

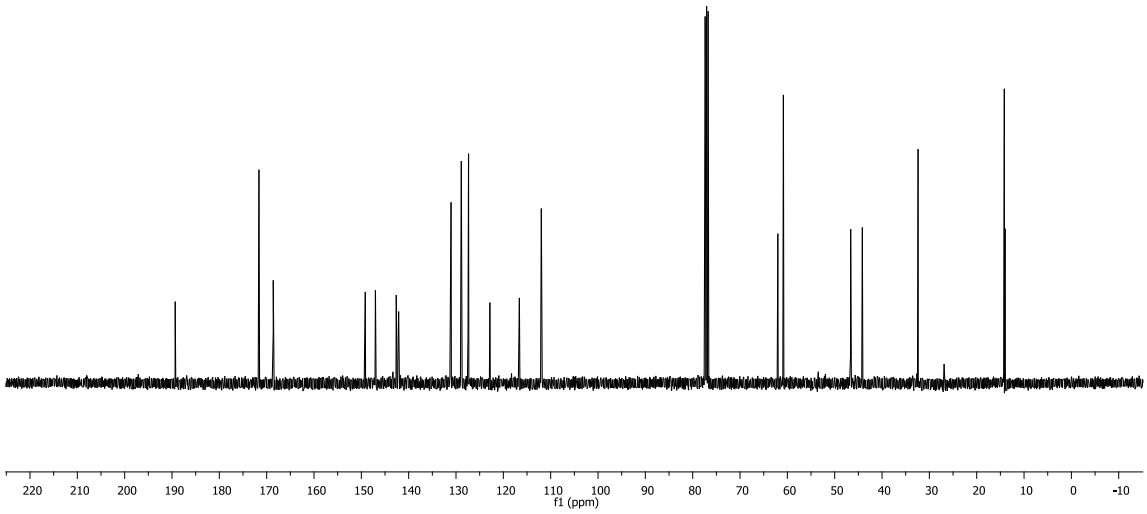

Diethyl 3,3'-((4-(3-(4-(N-(2-ethoxy-2-oxoethyl)sulfamoyl)phenyl)-1-(4-(((2,2,5-trimethyl-1,3-dioxan-5-yl)methoxy)sulfonyl)phenyl)-4,5-dihydro-1*H*-pyrazol-5-yl)phenyl)azanediyl)dipropanoate (5)

^{1}H NMR ($CDCl_3$, 400 MHz)

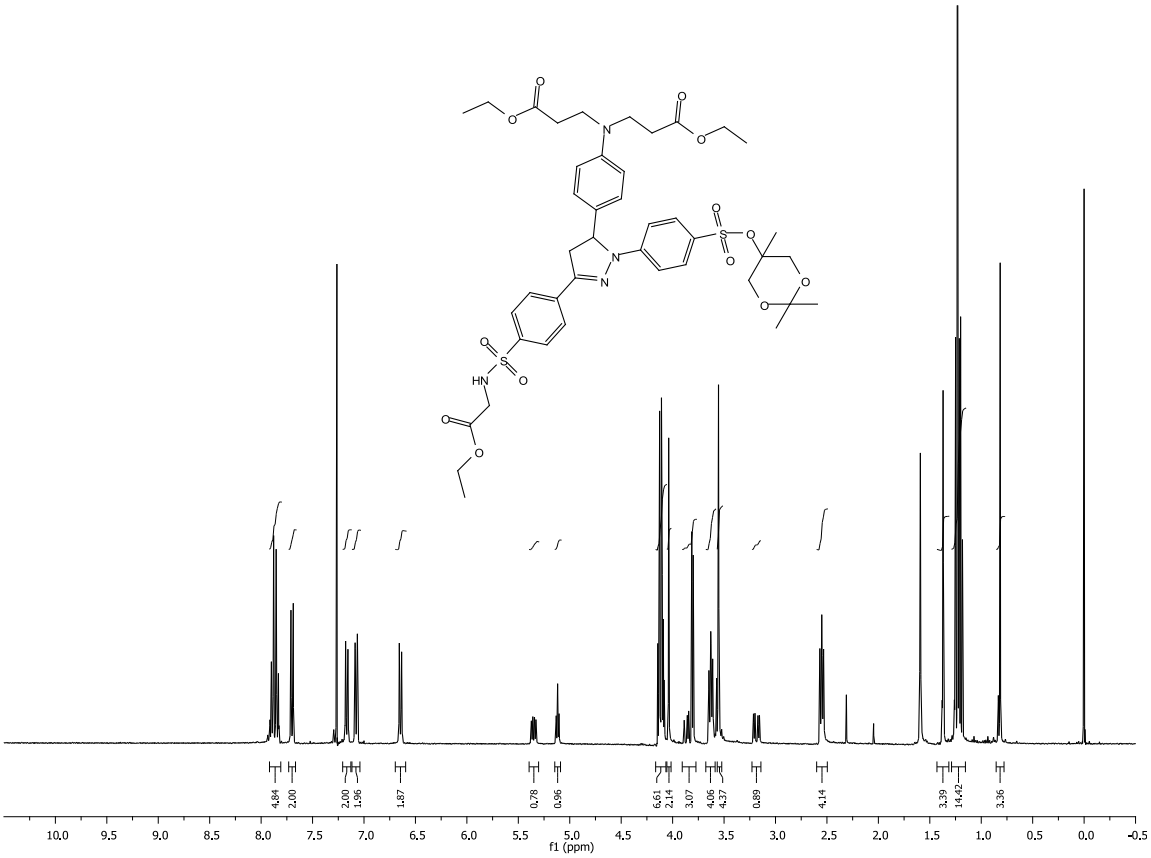

^{13}C NMR ($CDCl_3$, 400 MHz)

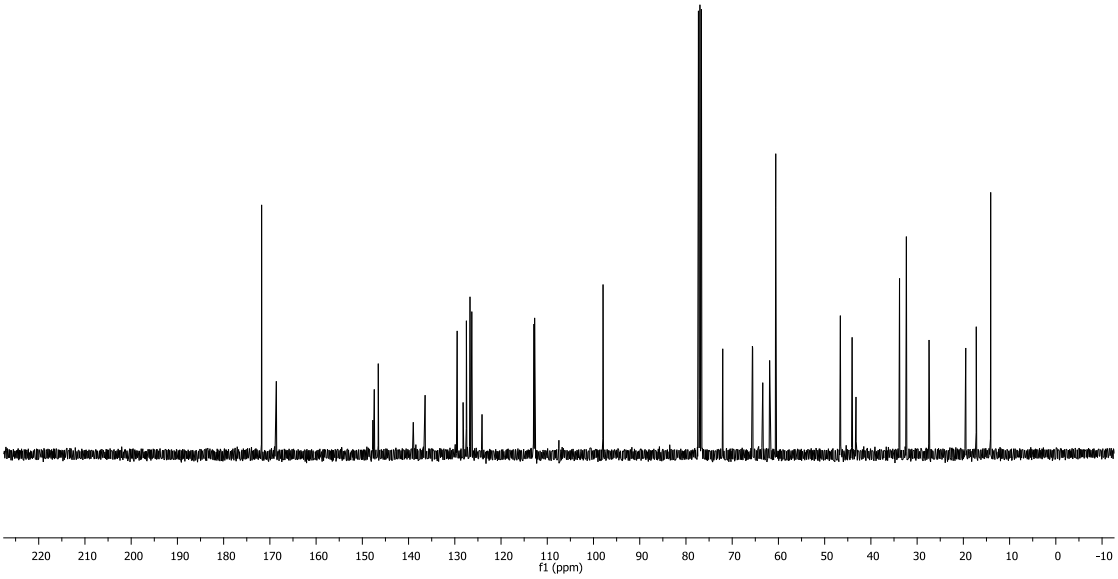

Diethyl 3,3'-((4-(3-(4-(N-(2-ethoxy-2-oxoethyl)-*N*-methylsulfamoyl)phenyl)-1-(4-(((2,2,5-trimethyl-1,3-dioxan-5-yl)methoxy)sulfonyl)phenyl)-4,5-dihydro-1*H*-pyrazol-5-yl)phenyl)azanediyl)dipropanoate (6)

^{1}H NMR ($CDCl_3$, 400 MHz)

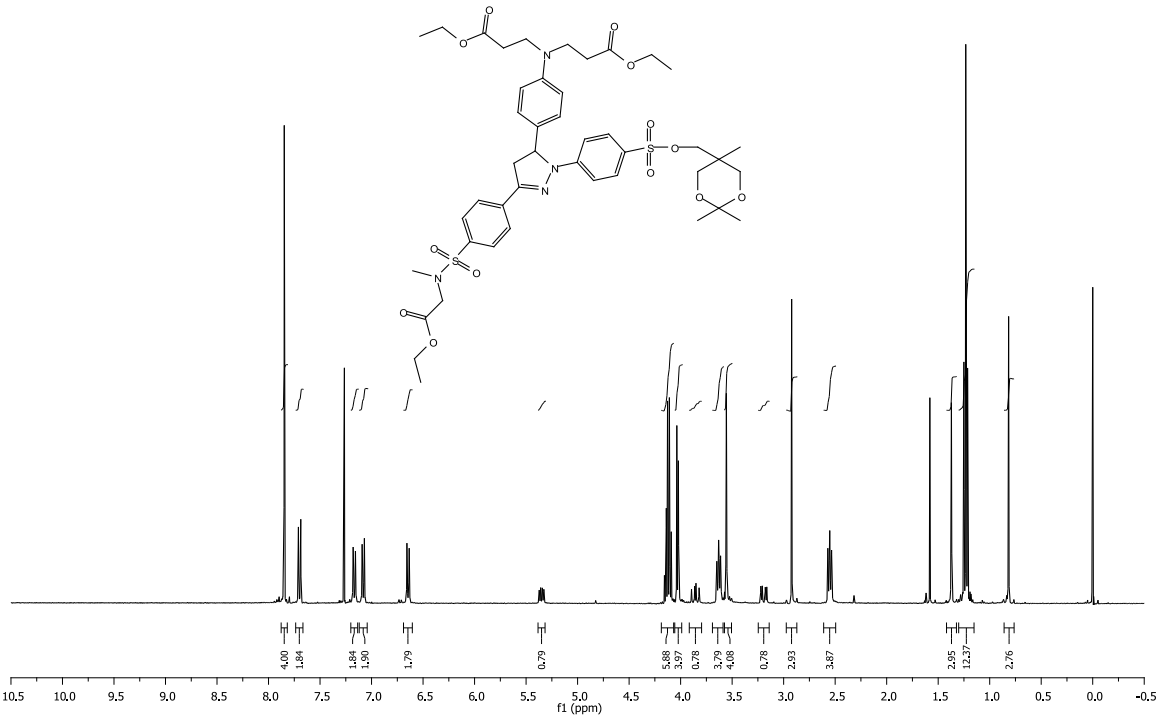

^{13}C NMR ($CDCl_3$, 400 MHz)

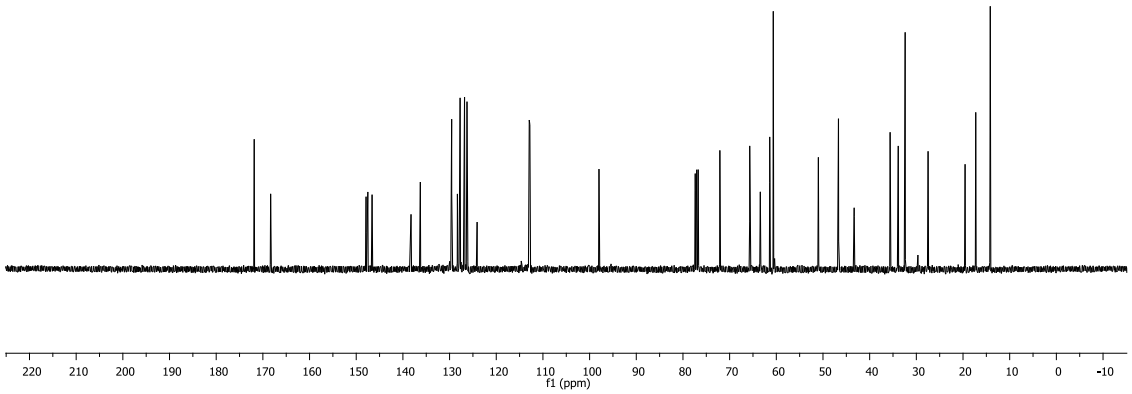

3,3'-((4-(3-(4-(*N*-(carboxymethyl)-*N*-methylsulfamoyl)phenyl)-1-(4-sulfophenyl)-4,5-dihydro-1*H*-pyrazol-5-yl)phenyl)azanediyl)dipropanoic acid (9)

^{1}H NMR (CD_3OD, 400 MHz)

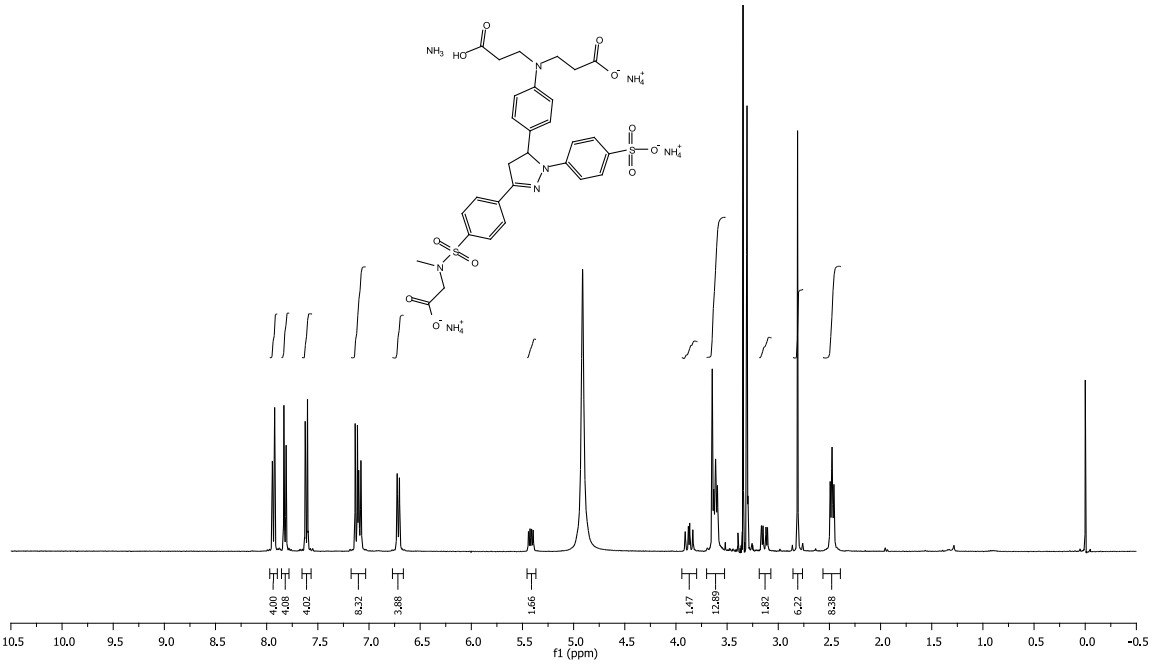

^{13}C NMR (CD_3OD, 400 MHz)

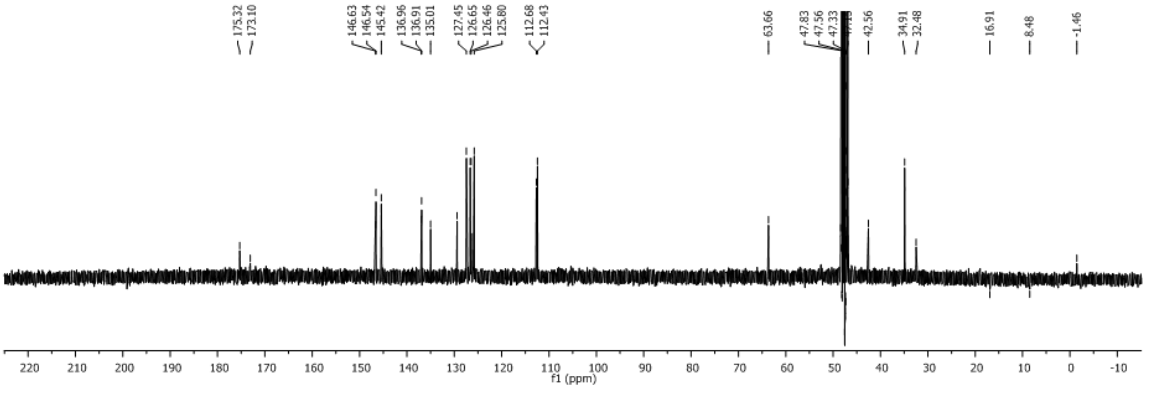

Diethyl 3,3'-((4-(3-(4-(N-(2-ethoxy-2-oxoethyl)-*N*-octylsulfamoyl)phenyl)-1-(4-(((2,2,5-trimethyl-1,3-dioxan-5-yl)methoxy)sulfonyl)phenyl)-4,5-dihydro-1*H*-pyrazol-5-yl)phenyl)azanediyl)dipropanoate (7)

^{1}H NMR ($CDCl_3$, 400 MHz)

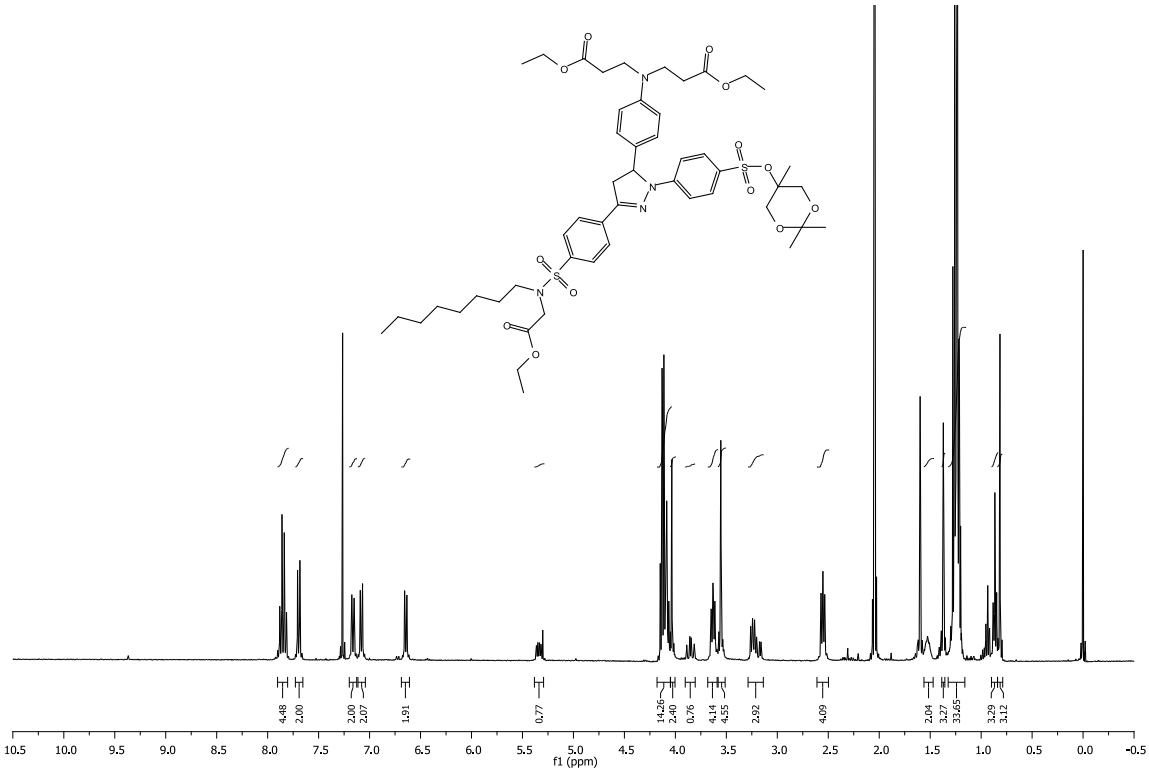

^{13}C NMR ($CDCl_3$, 400 MHz)

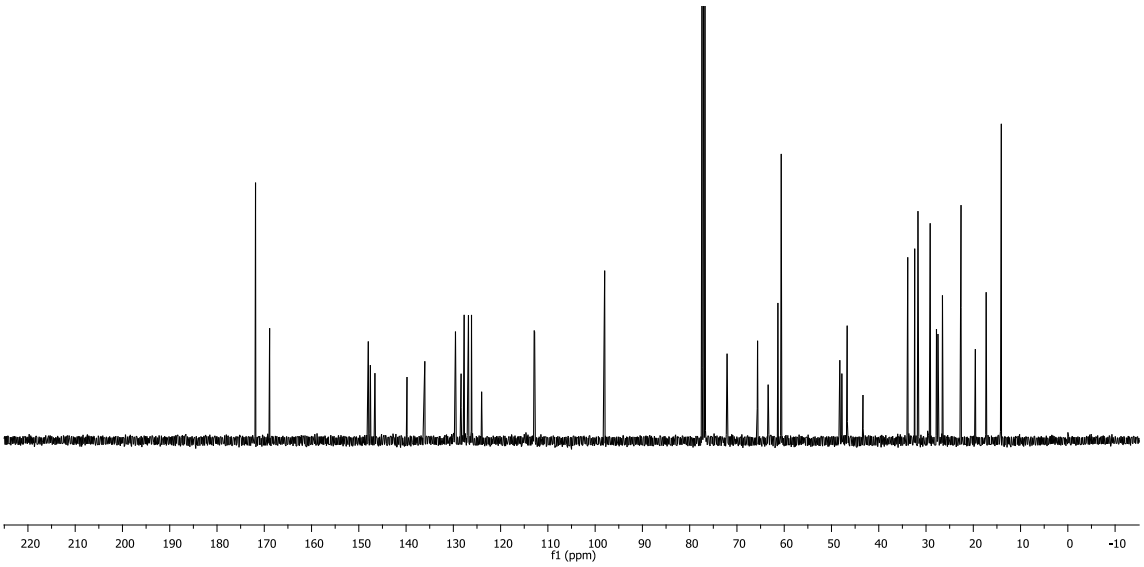

3,3'-((4-(3-(4-(*N*-(carboxymethyl)-*N*-octylsulfamoyl)phenyl)-1-(4-sulfophenyl)-4,5-dihydro-1*H*-pyrazol-5-yl)phenyl)azanediyl)dipropanoic acid (10)

^{1}H NMR (CD_3OD, 400 MHz)

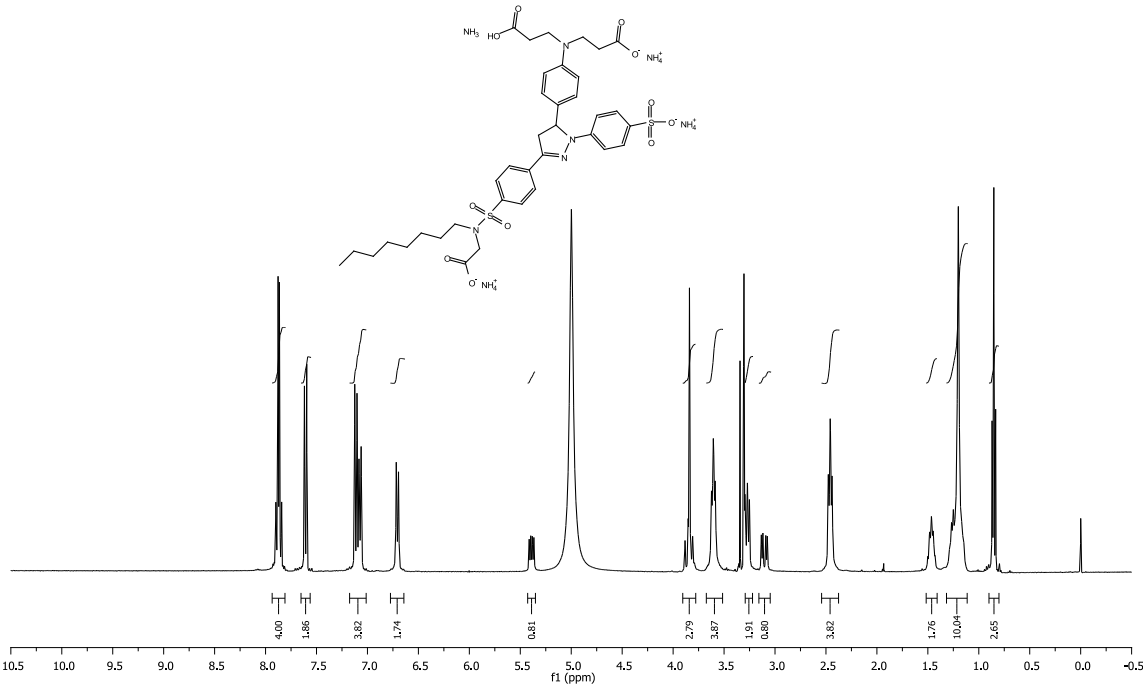

^{13}C NMR (CD_3OD, 400 MHz)

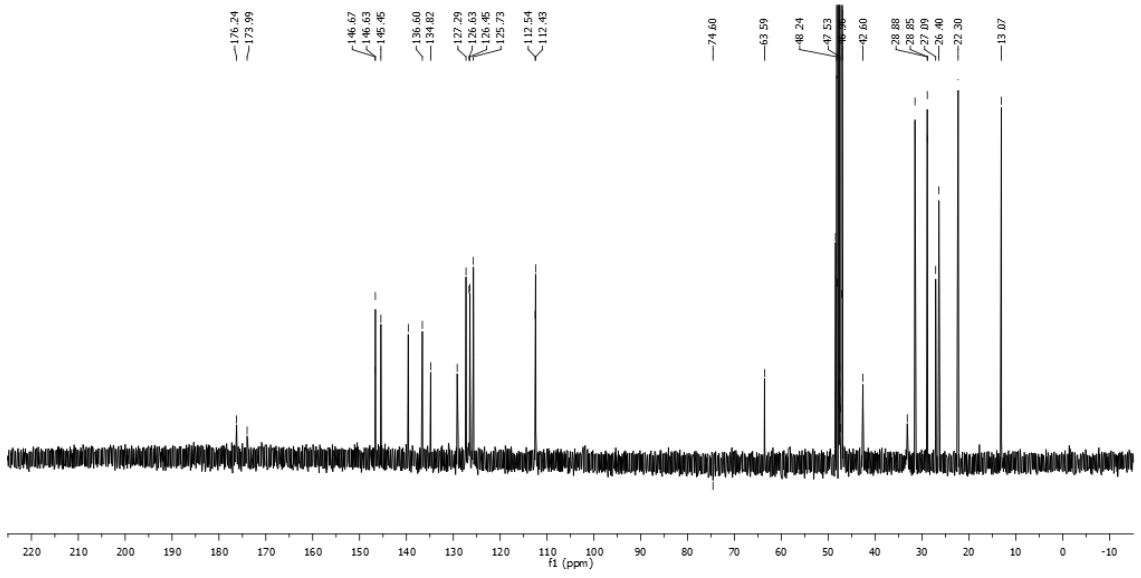

Diethyl 3,3'-((4-(3-(4-(*N*-(2-ethoxy-2-oxoethyl)-*N*-tetradecylsulfamoyl)phenyl)-1-(4-(((2,2,5-trimethyl-1,3-dioxan-5-yl)methoxy)sulfonyl)phenyl)-4,5-dihydro-1*H*-pyrazol-5-yl)phenyl)azanediyl)dipropanoate (8)

^{1}H NMR ($CDCl_3$, 400 MHz)

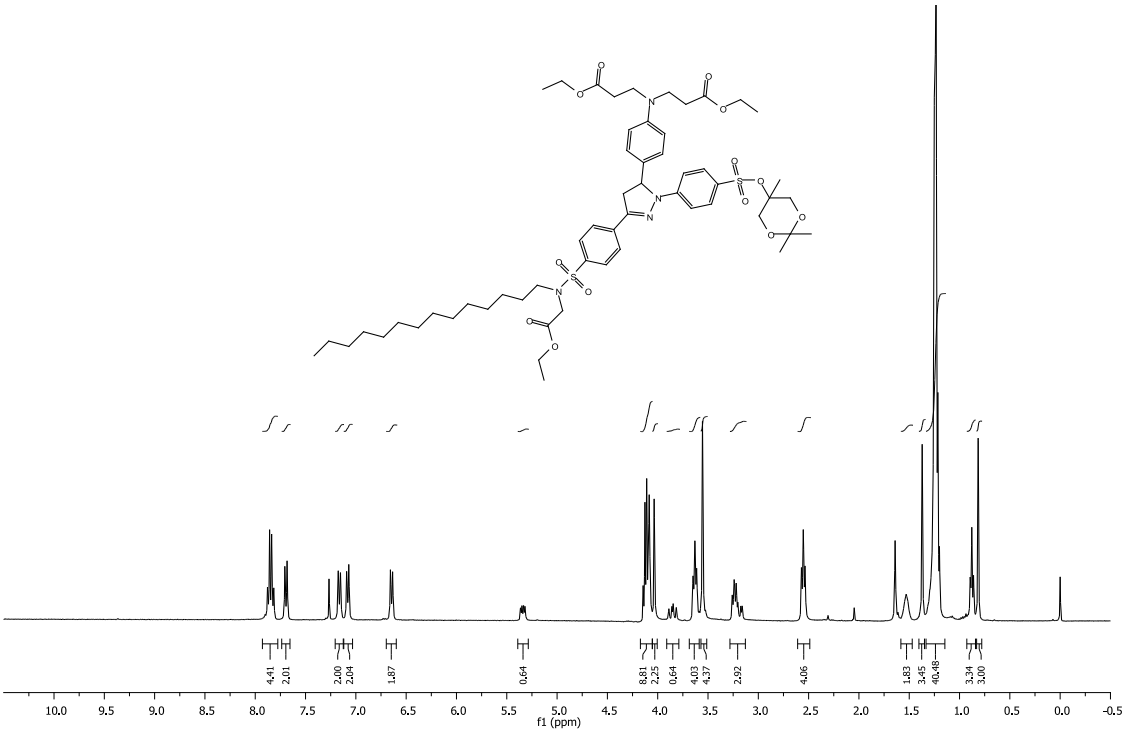

^{13}C NMR ($CDCl_3$, 400 MHz)

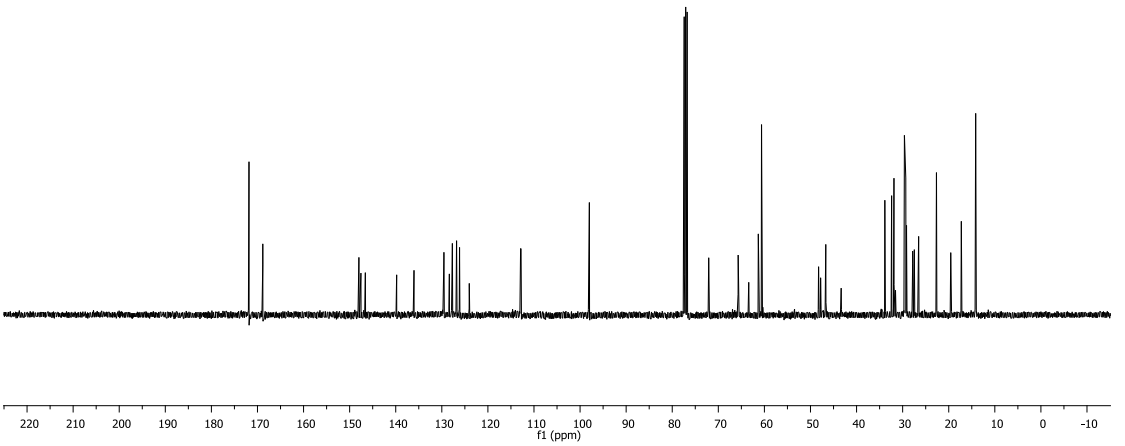

3,3'-((4-(3-(4-(*N*-(carboxymethyl)-*N*-tetradecylsulfamoyl)phenyl)-1-(4-sulfophenyl)-4,5-dihydro-1*H*-pyrazol-5-yl)phenyl)azanediyl)dipropanoic acid (11)

^{1}H NMR (CD_3OD, 400 MHz)

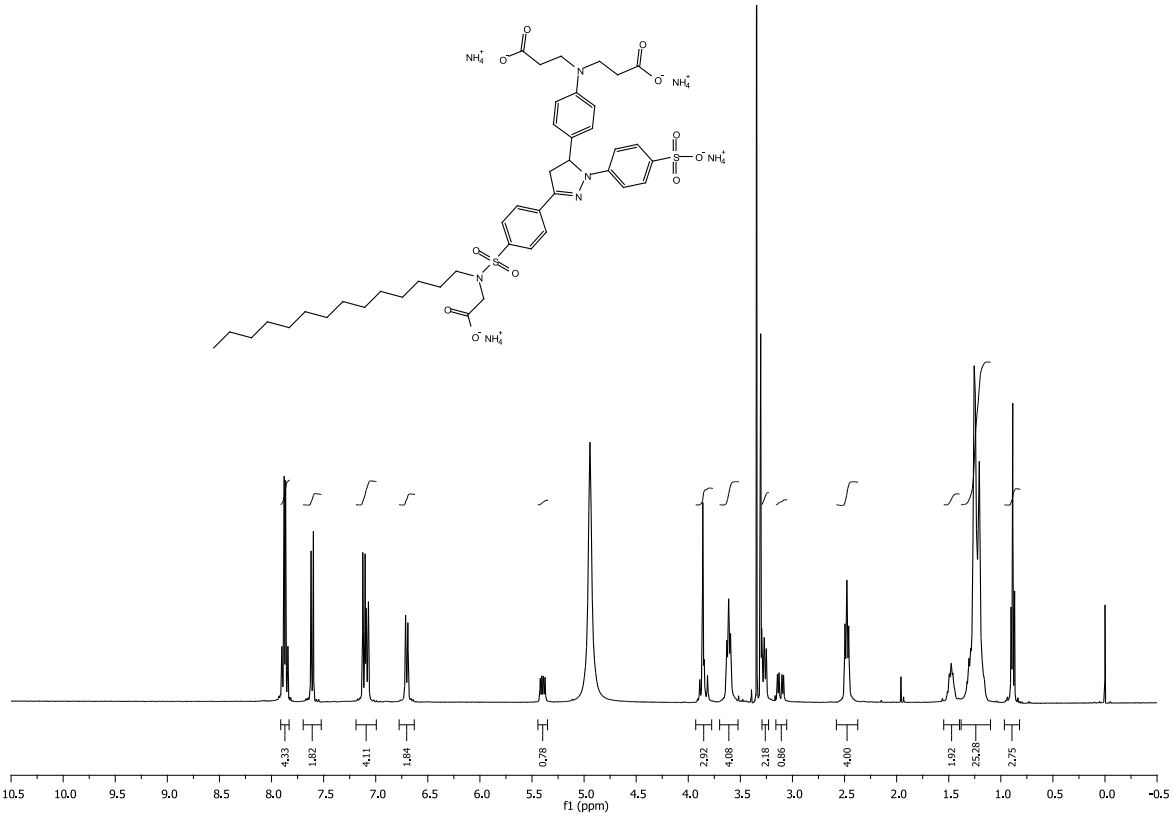

^{13}C NMR (CD_3OD, 400 MHz)

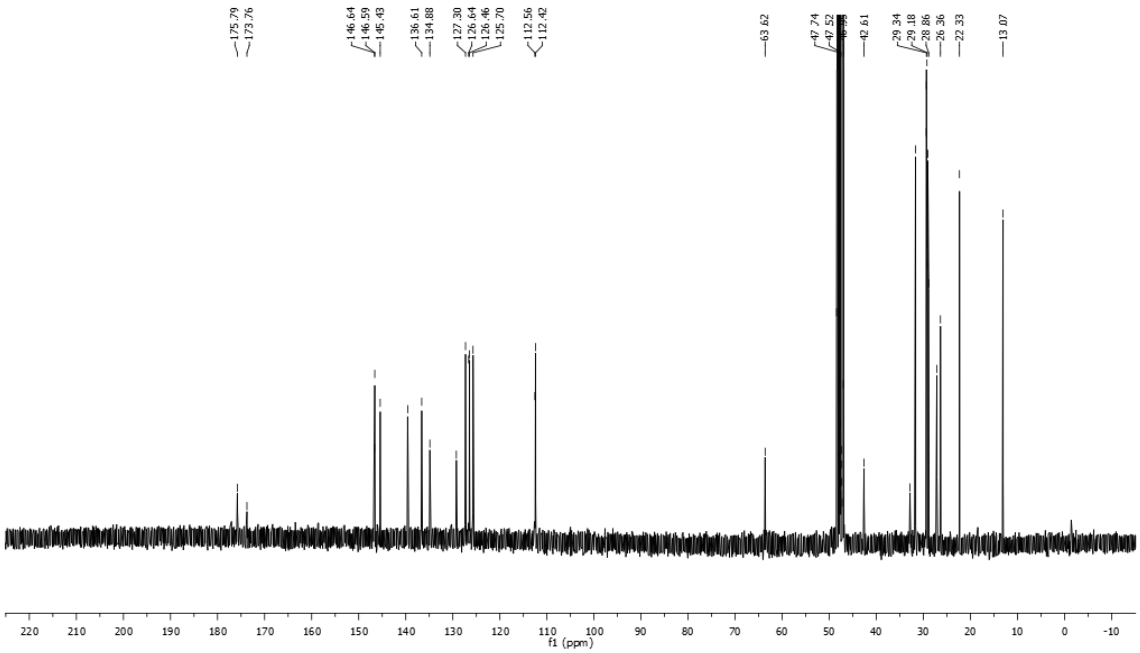

REFERENCES

1. Chaudhry, A. F.; Verma, M.; Morgan, M. T.; Henary, M. M.; Siegel, N.; Hales, J. M.; Perry, J. W.; Fahrni, C. J., Kinetically controlled photoinduced electron transfer switching in Cu(I)-responsive fluorescent probes. *Journal of the American Chemical Society* **2009,** *132* (2), 737-747.
2. Laubmann, K., *Chemische Berichte* **1888,** *21*, 1207.
3. (a) Verma, M.; Chaudhry, A. F.; Morgan, M. T.; Fahrni, C. J., Electronically tuned 1,3,5-triarylpyrazolines as Cu(I)-selective fluorescent probes. *Organic & Biomolecular Chemistry* **2010,** *8* (2), 363-370; (b) Cody, J.; Mandal, S.; Yang, L.; Fahrni, C. J., Differential tuning of the electron transfer parameters in 1,3,5-triarylpyrazolines: a rational design approach for optimizing the contrast ratio of fluorescent probes. *Journal of the American Chemical Society* **2008,** *130* (39), 13023-13032; (c) Fahrni, C. J., Design of cation-selective synthetic fluorescent indicators in chemosensors, John Wiley & Sons, Inc.: 2011; pp 371-394; (d) Fahrni, C. J.; Yang, L.; VanDerveer, D. G., Tuning the photoinduced electron-transfer thermodynamics in 1,3,5-triaryl-2-pyrazoline fluorophores: X-ray structures, photophysical characterization, computational analysis, and in vivo evaluation. *Journal of the American Chemical Society* **2003,** *125* (13), 3799-3812; (e) Morgan, M. T.; Bagchi, P.; Fahrni, C. J., Designed to dissolve: suppression of colloidal aggregation of Cu(I)-selective fluorescent probes in aqueous buffer and in-gel detection of a metallochaperone. *Journal of the American Chemical Society* **2011,** *133* (40), 15906-15909.

4. Rivett, D.; Rosevear, J.; Wilshire, J., The preparation and spectral properties of some monosubstituted 1,3,5,-Triphenyl-2-pyrazolines. *Australian Journal of Chemistry* **1979,** *32* (7), 1601-1612.

5. Fryhle C.; Solomon T. W. G., *Organic Chemistry*. 8 ed.; John Wiley & Sons, Inc.: The United States of America, 2004.

6. Gans, P.; O'Sullivan, B., GLEE, a new computer program for glass electrode calibration. *Talanta* **2000,** *51* (1), 33-37.

CHAPTER 3

LIPOSOME STUDIES AND DISCUSSION

3.1 Introduction

In 1972, Singer and Nicolson proposed the fluid mosaic model for characterizing the properties of biological membranes.[1] According to this model, biological membranes are analogous to a two-dimensional solution of proteins integrated within the viscous phospholipid bilayer solvent. Studies conducted around that time also showed that liposomes composed of phospholipids retained some of the main properties of biological membranes.[2] Since then, liposomes have been established as a versatile model system for studying the interactions between organic molecules and lipid bilayers. It is important to keep in mind that a system only composed of phospholipids is a greatly simplified representation of a biological membrane; nevertheless, it has been shown that liposomes containing cholesterol and a combination of structurally different phospholipids can effectively mimic lipid rafts regions, thus modeling biological membranes in a quite realistic way.[3]

The goal of this study was to investigate the effect of membrane proximity on the kinetics of the PET process of 1,3,5-triarylpyrazoline based fluorescence "turn-on" probes. Because a decrease in the PET kinetics results in a quantum yield increase, the photophysical properties provide a direct readout to gauge changes in the PET kinetics. Hence, fluorescence emission spectra and quantum yield measurements of pyrazolines **9-11** have been conducted in free aqueous buffer and in the presence of neutral and anionic liposomes as listed in Table 3.1.

Table 3.1: Emission and quantum yields of pyrazolines **9-11** in the presence and absence of liposomes

		emission$_{max}$[b] (nm)			**Φ[c]**		
compound[a]	**R**	**buffer[d]**	**neutral liposomes**	**anionic liposomes**	**buffer[d]**	**neutral liposomes**	**anionic liposomes**
9	CH_3	503	503	501	0.021	0.021	0.021
10	C_8H_{17}	500	500	498	0.023	0.024	0.023
11	$C_{14}H_{29}$	495	481	498	0.026	0.022	0.025

[a]Ammonium salt. [b]Samples were excited at 380 nm and emission was acquired over the range of 390-700 nm. [c]Quantum yield calculated based on a one point measurement compared to standard Norharmane in 0.1N H_2SO_4 as described in the experimental section. [d]10 mM MOPS/K^+ pH 7.2.

3.2 Liposome Studies

To study the effects of membrane proximity on the kinetics of the PET processes of 1,3,5 triarylpyrazoline based fluorescence probes, neutral liposomes composed of 1,2-dimyrisotyl-sn-glycero-3-phosphocholine and anionic liposomes composed of 1,2-dimyrisotyl-sn-glycero-3-phospho-(1'-rac-glycerol) as sodium salt, were used. Each sample contained 10 μM of the fluorescent probe and 200 μM of the lipid. Liposomes were created by the extrusion technique.[3b, 4] Briefly, the respective probe and the lipids were first combined in an organic solvent. After evaporating the solvent under reduced pressure, the solid residue was dried under high vacuum for 3 hours and then hydrated (swelled) by addition of 10 mM MOPS/K^+ buffer (pH 7.2). Each sample was vortexed to disperse the lipids and to form multilamellar vesicles. Finally, the multilamellar vesicles were extruded through a polycarbonate filter (pore size 100 nm) to give unilamellar vesicles.

3.2.1 Neutral Liposomes

Fluorescence emission spectra were acquired for pyrazolines **9**-**11** in the presence and absence of neutral liposomes as shown in Figure 3.1A-C. Pyrazolines **9** and **10**, containing a methyl and octyl group on the 3-aryl sulfonamide, respectively, exhibit neither changes in their fluorescence emission maximum nor the quantum yields (Figure 3.1 A and B). This result is expected for pyrazoline **9** since most likely an addition of one carbon cannot contribute enough lipophilic character to yield a favorable interaction with the liposome membrane. In case of pyrazoline **10**, it appears that even an 8-carbon alkyl chain does not provide sufficient lipophilicity for interacting with the neutral liposomes. Pyrazoline **11**, perhaps most surprisingly, showed neither an increase of the fluorescence intensity nor quantum yield as can be seen in Figure 3.1C; however, the peak emission wavelength shifted to higher energy from 495 nm to 481 nm, indicating some interaction with the liposome.

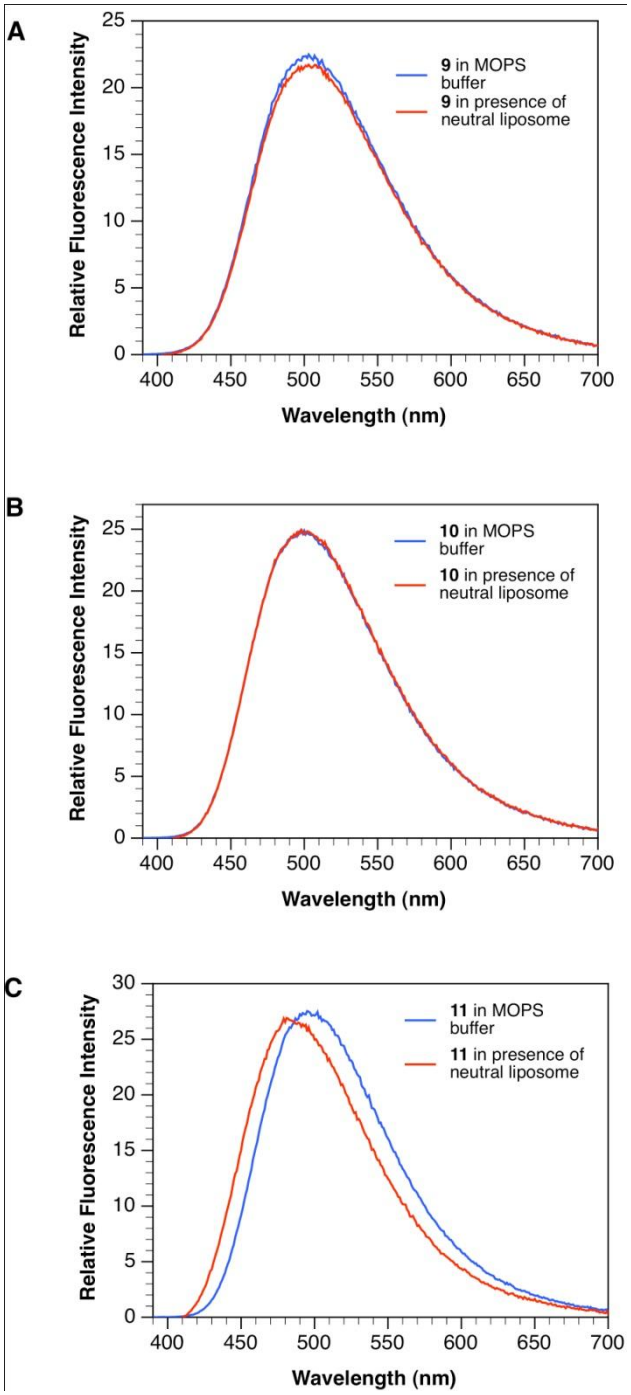

Figure 3.1: Fluorescence emission spectra of compounds **9-11** in presence and absence of neutral liposomes. Samples were excited at 380 nm and fluorescence emission was acquired over the range of 390-700 nm. Each sample containing 10 µM probe and 200 µM lipids was hydrated with a 10 mM MOPS/K^+ buffer (pH 7.2). Liposomes were made by an extrusion technique to give large unilamellar vesicles with an average diameter of 100 nm. All measurements were conducted at room temperature. Emission spectra were compared to the respective compound in 10 mM MOPS/K^+ buffer (pH 7.2). A. Fluorescence emission spectrum of pyrazoline **9.** B. Fluorescence emission spectrum of pyrazoline **10**. C. Fluorescence emission spectrum of pyrazoline **11**.

3.2.2 Anionic liposomes

Fluorescence emission spectra were acquired for pyrazolines **9**-**11** in the presence and absence of anionic liposomes as shown in Figure 3.2 A-C. Analogous to the behavior in the presence of neutral liposomes, pyrazolines **9** and **10** exhibit again neither changes in their fluorescence emission intensity nor their quantum yields (Figure 3.2A and B). This result is expected since there is repulsion between the overall anionic charge on the pyrazoline and the anionic phospholipids. In contrast, pyrazoline **11** showed, within experimental error, also no changes in the emission maximum (Figure 3.2C), presumably due to the unfavorable electrostatic repulsion of the polyanionic probe and the negatively charged liposome head groups.

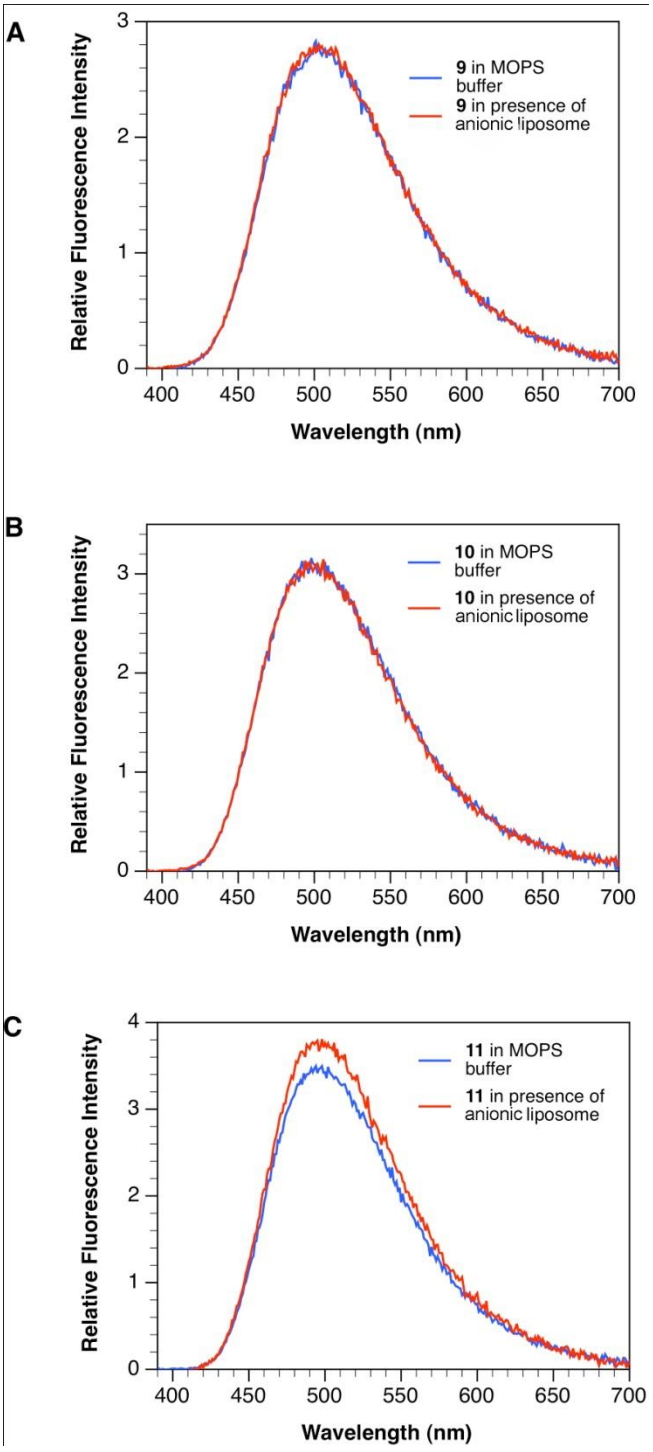

Figure 3.2: Fluorescence emission spectra of compounds **9-11** in presence and absence of anionic liposomes. Samples were excited at 380 nm and fluorescence emission was acquired over the range of 390-700 nm. Each sample containing 10 µM probe and 200 µM lipids was hydrated with a 10 mM MOPS/K^+ buffer (pH 7.2). Liposomes were made by an extrusion technique to give large unilamellar vesicles with an average diameter of 100 nm. All measurements were conducted at room temperature. Emission spectra were compared to the respective compound in 10 mM MOPS/K^+ buffer (pH 7.2). A. Fluorescence emission spectrum of pyrazoline **9.** B. Fluorescence emission spectrum of pyrazoline **10**. C. Fluorescence emission spectrum of pyrazoline **11**.

3.3 Conclusions

Pyrazolines **9-11** carry a net tetra-anionic charge, and, as outlined in the introduction to Chapter 2, the interaction with liposomes was expected to occur only through the alkylated sulfonamide moiety located on the 3-aryl ring. Upon equilibration of the probes with liposomal membranes, the polarity of the environment surrounding the probes was expected to change, due to increase in alkyl chain lengths, which should have resulted in differences in fluorescence intensity and quantum yield among the probes.

In summary, the results shown in Table 3.1, Figure 3.1 and Figure 3.2 indicate that membrane proximity had no significant effect on the fluorescence intensity or the quantum yields of pyrazolines **9-11**, a result that is surprisingly different from the initial observation made with **CTAP-2**. In view of the minor photophysical changes upon membrane anchoring, it should be therefore possible to design PET probes that selectively localize in biological membranes, for example in mitochondria or the Golgi apparatus, without suffering from environmentally dependent changes. Anchoring the probe in such a manner could then provide direct insights into the presence of specific analytes in these subcellular locations.

3.4 Future Directions

The results described above indicate that membrane proximity has negligible effect on the quantum yields and fluorescence intensities of pyrazolines **9-11**. To further characterize the effect of biological membranes on PET, perhaps a more complex composition of liposomes is required. Biological membranes are composed of three different types of amphipathic lipids; phospholipids, glycolipids and cholesterol. With regard to phospholipids, the chain length of the lipid tail may range from16 to 20 carbon atoms and the degree of saturation may further affect the physical properties of the membrane, mainly by changing its transition temperature which affects the fluidity of the lipid bilayer. Several studies were reported that describe the effect of cholesterol on membrane composition in liposomes, and the membrane structure indeed does become more complex, showing the presence of lipid rafts like regions along with liquid disordered and liquid ordered regions.[3b, 4]

The study presented herein is based on the interaction between pyrazolines **9-11** with liposomes as a function of different alkyl chain lengths. As explained above, the cell permeability experiment could not show a clear interaction between the compounds and the cells, though it is not clear to what extent the probes remained quenched and therefore not observable after cellular uptake. To ensure such interactions, a fluorescence "turn-on" probe could be linked either to the phospholipid head group or to its tail group. The latter could be achieved by click chemistry. A study conducted by Usoh et al.[5] modified a phospholipid tail by attaching an azide group to it. To investigate how the PET process is influenced by membrane embedment the pyrazoline could be utilized with an azide group as can be seen in Scheme 3.1.

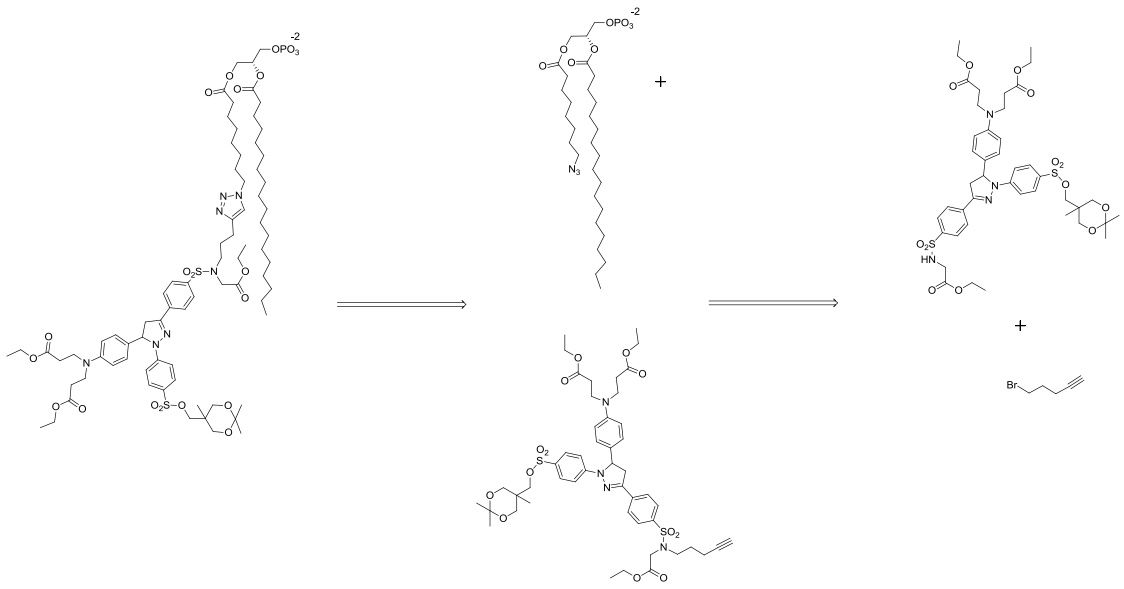

Scheme 3.1: Retrosynthetic analysis of a pyrazoline conjugated to a phospholipid.

In order to attach the probe to a phospholipid head group, a more sophisticated scheme is required. Several studies were conducted on attaching either a quenching moiety or a cargo moiety to a phospholipid.[6] Based on those studies, one way of attaching a pyrazoline probe to a phospholipid head group is by modifying a carboxylic acid group with an N-hydroxy succinimide activated ester, which would then be substituted by the phosphate group on the phospholipid. A retrosynthetic analysis for this procedure is presented in Scheme 3.2.

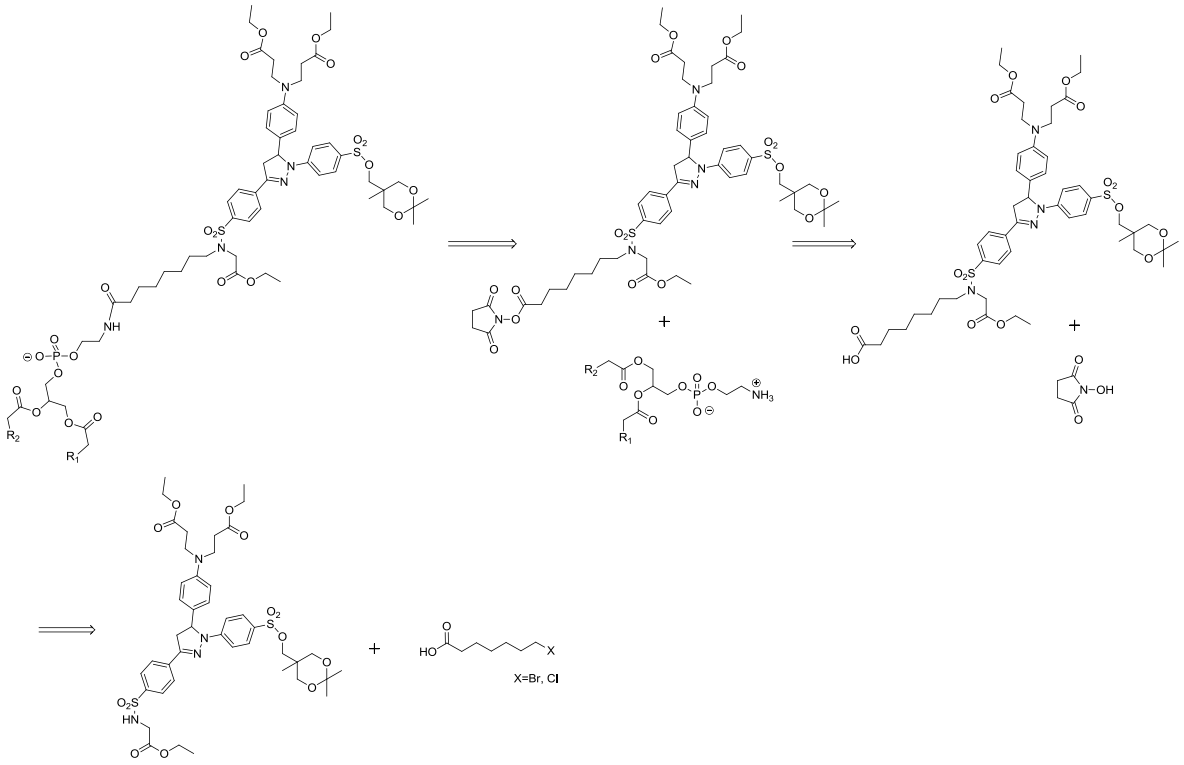

Scheme 3.2: Retrosynthetic analysis of a pyrazoline conjugated via head group of a phospholipid.

3.5 Material and methods

General: UV-vis absorption spectra were acquired at 22 °C with a Varian Cary Bio50 spectrophotometer with constant temperature accessory. Fluorescence spectra were recorded with a PTI fluorimeter. The fluorescence spectra were corrected for the spectral response of the detection system and for the spectral irradiance of the excitation source (via a calibrated photodiode). The path length was 1 cm for absorbance and fluorescence spectra and 10 cm for absorbance measurement for quantum yield determination.

3.5.1 Fluorescence absorbance and emission measurements

Fluorescence spectra were acquired with excitation at 380 nm and measured over the emission range of 390-700 nm, and the UV-vis absorbance was measured over the range of 250-500 nm.

3.5.2 Quantum Yields and Fluorescence Enhancement Factors

Quantum yield of compound **9** and fluorescence enhancement factor was determined in 0.1 M KCl, 10 mM MOPS buffer (pH 7.2), which had been filtered through a 0.45 μM membrane filter to remove dust particles. For quantum yield determination, excitation was at 380 nm and four data points with absorbances between 0.1 and 0.5 (l = 10 cm) were used. Norharmane was used as a standard with a known quantum yield of 58% in 0.1 M H_2SO_4. Equation 4.1 was used for a one point quantum yield determination in the case of liposome studies.

$$\Phi_x = \Phi_s \left(\frac{A_x}{A_s}\right)\left(\frac{I_x}{I_s}\right)\left(\frac{n_x}{n_s}\right)^2 \qquad (4.1)$$

Where Φ_x is the quantum yield of the unknown, Φ_s is the quantum yield of the standard, A_x is the optical density of the unknown, A_s is the optical density of the standard, I_x is the fluorescence intensity of the unknown, I_s is the fluorescence intensity of the standard and n_x is the refractive index of the medium of the unknown and n_s is the refractive index of the medium of the standard.

3.5.3 Liposome sample preparation[2]

All experiments were done using large unilamellar vesicles of 100 nm diameter of the appropriate phospholipids. All concentrations were adjusted for 3 mL final volume

and each sample contained 200 µM of lipids and 10 µM of compound. To each sample 60 µL of phospholipids (0.4 mg, 0.59 µmol for 1,2-dimyrisotyl-sn-glycero-3-phosphocholine and 0.4 mg, 0.58 µmol for 1,2-dimyrisotyl-sn-glycero-3-phospho-(1'-rac-glycero) sodium salt in chloroform was mixed with the appropriate volume of the compound in methanol. After drying the mixture first under a stream of N_2 and then under a high vacuum for 3 hours, it was hydrated (swelled) by adding 3.0 mL of 10 mM MOPS, 0.1 M KCl, pH 7.2 buffer and vortexed for 3 minutes to disperse the lipid and form homogeneous multilamellar vesicles. Large unilamellar vesicles were then prepared by extrusion technique. Briefly, the multilamellar vesicles were extruded through polycarbonate filters (pore diameter 100 nm) mounted in the extruder fitted with Hamilton syringes (Hamilton company, Reno, NV). The samples were subjected to 17 passes through the polycarbonate filter to give the final large unilamellar vesicles.

REFERENCES

1. Singer, S. J.; Nicolson, G. L., The fluid mosaic model of the structure of cell membranes. *Science* **1972,** *175* (4023), 720-731.
2. Sessa, G.; Weissmann, G., Effects of four components of the polyene antibiotic, Filipin, on phospholipid spherules (liposomes) and erythrocytes. *Journal of Biological Chemistry* **1968,** *243* (16), 4364-4371.
3. (a) Juhasz, J.; Davis, J. H.; Sharom, F. J., Fluorescent probe partitioning in giant unilamellar vesicles of 'lipid raft' mixtures. *Biochemical Journal* **2010,** *430* (3), 415-423; (b) Rukmini, R.; Rawat, S. S.; Biswas, S. C.; Chattopadhyay, A., Cholesterol organization in membranes at low concentrations: effects of curvature stress and membrane thickness. *Biophysical Journal* **2001,** *81* (4), 2122-2134.
4. Mukherjee, S.; Raghuraman, H.; Chattopadhyay, A., Membrane localization and dynamics of Nile Red: effect of cholesterol. *Biochimica et Biophysica Acta (BBA) Biomembranes* **2007,** *1768* (1), 59-66.
5. Usoh, C. O., Synthesis of tagged phospholipid analogs for studying protein-lipid binding. *University of Tennessee Honors Thesis Projects* **2007**.
6. (a) Kondo, M.; Mehiri, M.; Regen, S. L., Viewing membrane-bound molecular umbrellas by Parallax analyses. *Journal of the American Chemical Society* **2008,** *130* (41), 13771-13777; (b) Gabizon, A.; Shmeeda, H.; Horowitz, A. T.; Zalipsky, S., Tumor cell targeting of liposome-entrapped drugs with phospholipid-anchored folic acid–PEG conjugates. *Advanced Drug Delivery Reviews* **2004,** *56* (8), 1177-1192.